Plant Communications
Research article

CellPress
Partner Journal

Clathrin light chains negatively regulate plant immunity by hijacking the autophagy pathway

Hu-Jiao Lan[1,9], Jie Ran[1,9], Wen-Xu Wang[1,9], Lei Zhang[1], Ni-Ni Wu[1], Ya-Ting Zhao[1], Min-Jun Huang[1], Min Ni[1], Fen Liu[7], Ninghui Cheng[8], Paul A. Nakata[8], Jianwei Pan[3], Steven A. Whitham[4], Barbara J. Baker[5,6] and Jian-Zhong Liu[1,2,*]

[1]Zhejiang Provincial Key Laboratory of Biotechnology on Specialty Economic Plants, Zhejiang Normal University, Jinhua 321004, China

[2]Institute of Plant Genetics and Developmental Biology, College of Chemistry and Life Sciences, Zhejiang Normal University, Jinhua 321004, China

[3]College of Life Sciences, Lanzhou University, Lanzhou 730000, China

[4]Department of Plant Pathology and Microbiology, Iowa State University, Ames, IA 50011, USA

[5]Department of Plant and Microbial Biology, University of California, Berkeley, Berkeley, CA 94720, USA

[6]Plant Gene Expression Center, U.S. Department of Agriculture-Agricultural Research Service, Albany, CA 94706, USA

[7]Lushan Botanical Garden, Chinese Academy of Sciences, Jiujiang 332000, China

[8]U.S. Department of Agriculture-Agricultural Research Service, Children's Nutrition Research Center, Department of Pediatrics, Baylor College of Medicine, Houston, TX 77030, USA

[9]These authors contributed equally to this article.

***Correspondence: Jian-Zhong Liu (jzliu@zjnu.cn)**

https://doi.org/10.1016/j.xplc.2024.100937

ABSTRACT

The crosstalk between clathrin-mediated endocytosis (CME) and the autophagy pathway has been reported in mammals; however, the interconnection of CME with autophagy has not been established in plants. Here, we report that the *Arabidopsis* CLATHRIN LIGHT CHAIN (CLC) subunit 2 and 3 double mutant, *clc2-1 clc3-1*, phenocopies *Arabidopsis* AUTOPHAGY-RELATED GENE (*ATG*) mutants in both autoimmunity and nutrient sensitivity. Accordingly, the autophagy pathway is significantly compromised in the *clc2-1 clc3-1* mutant. Interestingly, multiple assays demonstrate that CLC2 directly interacts with ATG8h/ATG8i in a domain-specific manner. As expected, both GFP-ATG8h/GFP-ATG8i and CLC2-GFP are subjected to autophagic degradation, and degradation of GFP-ATG8h is significantly reduced in the *clc2-1 clc3-1* mutant. Notably, simultaneous knockout of *ATG8h* and *ATG8i* by CRISPR-Cas9 results in enhanced resistance against *Golovinomyces cichoracearum*, supporting the functional relevance of the CLC2–ATG8h/8i interactions. In conclusion, our results reveal a link between the function of CLCs and the autophagy pathway in *Arabidopsis*.

Key words: autophagy, clathrin light chain, immunity, clathrin-mediated endocytosis, senescence, cell death

Lan H.-J., Ran J., Wang W.-X., Zhang L., Wu N.-N., Zhao Y.-T., Huang M.-J., Ni M., Liu F., Cheng N., Nakata P.A., Pan J., Whitham S.A., Baker B.J., and Liu J.-Z. (2024). Clathrin light chains negatively regulate plant immunity by hijacking the autophagy pathway. Plant Comm. **5**, 100937.

INTRODUCTION

Clathrin-mediated endocytosis (CME) plays critical roles in internalization and recycling of plasma membrane (PM)-localized proteins (Wang et al., 2013; Hao et al., 2014). Clathrin is a complex of triskelion shape that consists of three heavy chains and three light chains (Chen et al., 2011). The *Arabidopsis thaliana* genome encodes two *CLATHRIN HEAVY CHAIN* (*CHC*) and three *CLATHRIN LIGHT CHAIN* (*CLC*) genes (Chen et al., 2011). Loss of *CLC2* and *CLC3* leads to impaired auxin-regulated endocytosis of PIN proteins and consequently to pleiotropic developmental defects, including partial male sterility (Wang et al., 2013). PM cargo proteins are usually mono-ubiquitinated prior to CME (Khaled et al., 2015). The mono-ubiquitinated proteins are first internalized in clathrin-coated vesicles (CCVs) to the *trans*-Golgi network (TGN)/early endosomes (EE), where endocytic and exocytotic/secretion pathways converge (Viotti et al., 2010). Subsequently, cargo proteins are sorted into the intralumenal

Published by the Plant Communications Shanghai Editorial Office in association with Cell Press, an imprint of Elsevier Inc., on behalf of CSPB and CEMPS, CAS.

vesicles of multivesicular bodies (MVBs) and finally fused with vacuoles with the assistance of the ENDOSOMAL SORTING COMPLEX REQUIRED FOR TRANSPORT (ESCRT) machinery (Khaled et al., 2015; Rodriguez-Furlan et al., 2019). Alternatively, these cargo proteins coated on the CCVs are deubiquitinated and recycled back to the PM from the TGN/EE (Khaled et al., 2015; Paez et al., 2016). Consistent with these observations, recent studies have provided genetic evidence that clathrin function is required not only for endocytosis but also for exocytosis and post-Golgi trafficking (Larson et al., 2017; Yan et al., 2021).

Macroautophagy (hereafter referred to as autophagy) is an evolutionarily conserved catabolic process in which damaged or no-longer-needed cytoplasmic components are engulfed into double-membrane vesicles called autophagosomes for vacuole/lysosome degradation (Li and Vierstra, 2012). Autophagic degradation can be either non-selective or selective. Under conditions of senescence and nutrient deprivation, proteins, carbohydrates, and lipids can be broken down non-selectively via bulk autophagy to replenish the cells with carbon and nitrogen needed for survival and new growth (Li and Vierstra, 2012; Liu and Bassham, 2012). On the other hand, aggregated proteins, damaged organelles induced under stress conditions, or even invading pathogens can be cleared by selective autophagy. In this case, lipidated AUTOPHAGY-RELATED GENE 8 (ATG8) proteins anchored on the autophagosomal membrane recruit cargoes to autophagosomes by interacting with ATG8-interacting motif (AIM)-containing cargo receptors (the core AIM sequence is defined as W/F/Y-XX-L/I/V) (Noda et al., 2010; Li and Vierstra, 2012). An LIR/AIM docking site (LDS) within the ATG8 amino acid sequence is responsible for interaction with cargo receptors (Yamaguchi et al., 2010; Marshall et al., 2019).

Nine ATG8 isoforms have been identified in *Arabidopsis* (Kellner et al., 2017). Plant ATG8 genes are grouped into two clades by phylogenetic analysis (Kellner et al., 2017). The C terminus of newly synthesized ATG8s in clade I (ATG8a to ATG8g) is cleaved by ATG4, resulting in an exposed Gly residue at the C terminus. The lipid molecule phosphatidylethanolamine (PE) is then conjugated to the exposed Gly residue of ATG8 with the sequential assistance of the E1-like enzyme ATG7 and the E2-like enzyme ATG3 (Ohsumi, 2001; Seo et al., 2016). ATG8-PE is targeted to a pre-autophagosomal structure, where it plays a role in autophagosome formation. The clade II isoforms (ATG8h and ATG8i) lack extra amino acid residues at the C terminus after the glycine residue, indicating that ATG8h and ATG8i proteins can be lipidated and anchored to the autophagosome membrane without ATG4 processing (Seo et al., 2016).

Both pro- and anti-cell-death functions have been linked to autophagy (Liu et al., 2005; Patel et al., 2008; Hofius et al., 2009; Yoshimoto et al., 2009; Üstün and Hofius, 2018). Silencing of ATG6/Beclin1 leads to unrestricted spread of cell death beyond the sites of TMV infection on leaves of *Nicotiana benthamiana* plants expressing the *N* gene (Liu et al., 2005), whereas HR triggered by RPS4 and RPM1 is compromised in *atg* mutants (Hofius et al., 2009). In addition, autoimmune phenotypes of chlorotic cell death/accelerated senescence are observed in different *atg* mutants (Yoshimoto et al., 2009; Wang et al., 2011; Üstün and Hofius, 2018).

Here, we show that loss of function of CLC2 and CLC3 in *Arabidopsis* leads to chlorotic cell death/accelerated senescence resulting from elevated accumulation of both reactive oxygen species (ROS) and salicylic acid (SA). In addition, we provide genetic evidence that ROS and SA form a positive feedback loop that amplifies autoimmune signals and that both ROS and SA are essential for the autoimmune phenotype of the *clc2-1 clc3-1* plants. Unexpectedly, we found that loss of CLC2 and CLC3 impaired autophagy, which may account for the autoimmune phenotype of the *clc2-1 clc3-1* mutant. Notably, we provide evidence that CLC2 directly interacts with the Clade II ATG8 proteins, ATG8h and ATG8i, in an AIM1- and LDS-dependent manner. Furthermore, we show that GFP-ATG8h/GFP-ATG8i and CLC2-GFP are subject to autophagic degradation in the vacuoles. Finally, we show that simultaneous knockout of ATG8h and ATG8i results in enhanced resistance against *Golovinomyces cichoracearum*, highlighting the functional relevance of the CLC2–ATG8h/8i interactions. Taken together, our results reveal a previously unidentified link between CLC function and autophagy in plants.

RESULTS

Loss of *CLC2* and *CLC3* in *Arabidopsis* results in SA- and H_2O_2-dependent activation of defense responses

While investigating the roles of the CLCs in endocytosis of auxin efflux carriers (Wang et al., 2013; Zhang et al., 2017), we unexpectedly found that accelerated senescence and/or spontaneous cell death occurred in the leaves of the *clc2-1 clc3-1* double-mutant plants (compare Figure 1A and 1B, see arrows in Figure 1B). This cell death was confirmed by trypan blue staining (compare Figure 1C and 1D, see arrows in Figure 1D). Spontaneous cell death in plants is usually induced by over-accumulation of H_2O_2 (Lamb and Dixon, 1997). Consistent with this scenario, H_2O_2 accumulation was significantly higher in leaves of the *clc2-1 clc3-1* double-mutant plants than in equivalent leaves of wild-type Col-0 plants (compare Figure 1E and 1F, see arrows in Figure 1F).

SA is a potent cell-death inducer and interacts synergistically with H_2O_2 to induce cell death (Shirasu et al., 1997; Yoshimoto et al., 2009; Xu et al., 2018). As expected, both free SA and total SA levels were significantly higher in leaves of the *clc2-1 clc3-1* double-mutant plants than in those of Col-0 plants, especially in the leaves with cell death (Figure 1G and 1H). Together, these results indicate that the accelerated senescence and/or cell death observed in the *clc2-1 clc3-1* plants is correlated with over-accumulation of both H_2O_2 and SA.

Consistent with the enhanced H_2O_2 and SA levels, expression of *PATHOGENESIS-RELATED GENE 1* (*PR1*) was induced to a much higher level in *clc2-1 clc3-1* mutant plants than in Col-0 plants (Figure 1I). Accordingly, the *clc2-1 clc3-1* mutant plants displayed enhanced resistance against *Pseudomonas syringae* pv. *tomato* DC3000 (*Pst* DC3000) relative to Col-0 plants (Figure 1J). These results indicate that loss of CLC2 and CLC3

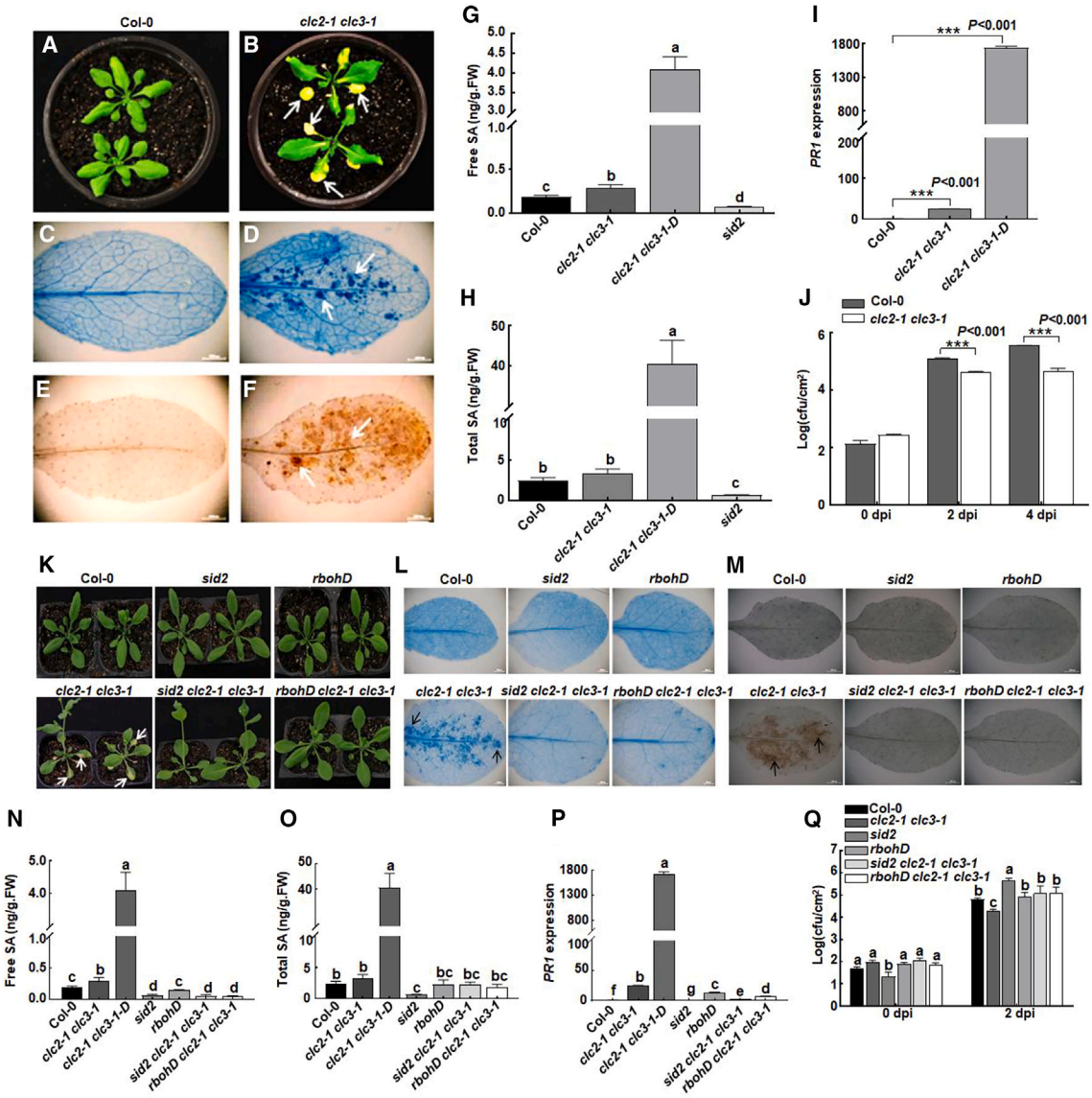

Figure 1. Defense responses activated in the *clc2-1 clc3-1* mutant are dependent on SA and H_2O_2.

(A) Twenty-one-day-old wild-type Col-0 plants.

(B) Twenty-one-day-old *clc2-1 clc3-1* double-mutant plants. Accelerated senescence and chlorotic cell death are indicated by the white arrows.

(C) Col-0 leaf stained with trypan blue.

(D) *clc2-1 clc3-1* leaf stained with trypan blue. The white arrows point to intensely stained areas with cell death.

(E) Col-0 leaf stained with DAB.

(F) *clc2-1 clc3-1* leaf stained with DAB. The white arrows point to regions of H_2O_2 accumulation.

(G and H) Increased accumulation of free SA **(G)** and total SA **(H)** in *clc2-1 clc3-1* double-mutant plants relative to Col-0 plants. *clc2-1 clc3-1-D* represents the mutant plants with cell death on the leaves.

(I) Expression of *PR1* was highly induced in the *clc2-1 clc3-1* double mutant relative to Col-0. *ACTIN2* (At3G18780) was used as the endogenous reference gene.

(J) The *clc2-1 clc3-1* double-mutant plants displayed enhanced resistance against *Pseudomonas syringae* pv. *tomato* DC3000 (*Pst* DC3000).

(K) Twenty-one-day-old wild-type Col-0 plants and various indicated mutant plants. White arrows point to the areas with accelerated senescence/cell death.

(L) Trypan-blue-stained leaves of wild-type Col-0 and the indicated mutant plants. The black arrows point to areas with cell death.

(M) DAB-stained leaves of wild-type Col-0 and the indicated mutant plants. The black arrows point to the areas of H_2O_2 accumulation.

(N–P) Levels of free SA **(N)** and total SA **(O)** and the expression of *PR1* mRNA **(P)** in wild-type Col-0 and various indicated mutant plants. *ACTIN2* (At3G18780) was used as the endogenous reference gene.

(Q) Growth of *Pst* DC3000 in wild-type Col-0 and the indicated mutants at 0 and 2 days post-inoculation (dpi). Asterisks in **(C)**, **(F)**, and **(G)** indicate significant differences (ns, no significant change; $*p < 0.05$; $**p < 0.01$; $***p < 0.001$, two-tailed unpaired *t*-test). Different letters in **(N)** to **(Q)** indicate significant differences at $p < 0.05$ (one-way ANOVA with *post hoc* Duncan's test). These experiments were repeated three times with similar results.

function in *Arabidopsis* results in SA- and H_2O_2-associated cell death and activated immunity.

Loss of function of either ISOCHORISMATE SYNTHASE 1 or RESPIRATORY BURST OXIDASE HOMOLOG PROTEIN D rescues the autoimmune phenotypes of *clc2-1 clc3-1* double-mutant plants

SALICYLIC ACID INDUCTION DEFICIENT 2 (*SID2*) encodes the key enzyme ISOCHORISMATE SYNTHASE 1 (ICS1), which converts isochorismate to chorismate in the chloroplast and is responsible for 90% of pathogen-induced SA biosynthesis in *Arabidopsis* (Wildermuth et al., 2001). RESPIRATORY BURST OXIDASE HOMOLOG PROTEIN D (RBOHD) is responsible for pathogen-induced H_2O_2 production (Torres et al., 2002). To genetically dissect the signaling pathways involved in the autoimmune phenotypes of the *clc2-1 clc3-1* mutant, we generated the *sid2 clc2-1 clc3-1* and *rbohD clc2-1 clc3-1* triple mutants by genetic crossing. Interestingly, a deficiency of either *SID2* or *RBOHD* could rescue almost all the autoimmune phenotypes of the *clc2-1 clc3-1* mutant plants, including accelerated senescence or spontaneous cell death (Figure 1K and 1L), enhanced accumulation of H_2O_2 (Figure 1M) and SA (Figure 1N and 1O), induced expression of *PR1* (Figure 1P), and enhanced bacterial resistance (Figure 1Q). These results provide strong evidence that SA and ROS form a positive feedback loop that initiates and amplifies immunity-related signals. The concomitant presence of both SA and H_2O_2 is required for the autoimmune responses observed in the *clc2-1 clc3-1* double-mutant plants.

The *clc2-1 clc3-1* double-mutant phenocopies the *atg2-1* mutant

The autoimmune phenotypes of the *clc2-1 clc3-1* mutant (Figure 1) have also been observed in many *atg* mutants (Yoshimoto et al., 2009; Lenz et al., 2011; Üstün and Hofius, 2018). The similarities between the *clc2-1 clc3-1* and *atg* mutants raise the possibility that clathrin function is somehow associated with autophagy. To test this possibility, we compared the phenotypes of the *atg2-1* mutant with those of the *clc2-1 clc3-1* mutant side-by-side. We found that the *atg2-1* mutant plants displayed accelerated senescence and cell-death phenotypes similar to those of *clc2-1 clc3-1* (Supplemental Figure 1A and 1B). Likewise, H_2O_2 was over-accumulated in both the *atg2-1* and the *clc2-1 clc3-1* mutant plants (Supplemental Figure 1C). It is well documented that the autoimmune phenotypes of many *atg* mutants are SA-dependent (Yoshimoto et al., 2009; Lenz et al., 2011; Üstün and Hofius, 2018) and that SA shows greater accumulation in *atg* mutants than in Col-0 (Yoshimoto et al., 2009; Lenz et al., 2011). Together, these results suggest that loss of *CLC2* and *CLC3* might have a negative effect on the autophagy pathway in *Arabidopsis*.

The *clc2-1 clc3-1* and *atg2-1* mutants display similar enhanced sensitivity to carbon and nitrogen starvation

A hallmark of autophagy deficiency is enhanced sensitivity to carbon (C) or nitrogen (N) starvation (Li and Vierstra, 2012). To test whether the *clc2-1 clc3-1* mutant was sensitive to N or C starvation, we performed N or C deprivation assays using seedlings of the indicated genotypes. The typical yellowish phenotype that indicated enhanced sensitivity to either C or N starvation was observed for both the *clc2-1 clc3-1* and the *atg2-1* seedlings but less so for the Col-0 seedlings (Figure 2A). We next obtained detached leaves from the same positions on 4-week-old plants of the indicated genotypes and kept them in the dark for 6 days. Accelerated senescence was observed for the dark-treated *clc2-1 clc3-1* and *atg2-1* mutant leaves but not for the dark-treated Col-0 leaves (Figure 2B). Chlorophyll content measurements were highly correlated with the chlorotic phenotypes in these lines (Figure 2C). Collectively, these data indicate that autophagy is likely compromised in the *clc2-1 clc3-1* mutant.

The *clc2-1 clc3-1* mutant exhibits enhanced resistance against the fungal pathogen *G. cichoracearum* and the bacterial pathogen *Pst DC3000*

atg2-1 mutant plants have been reported to display enhanced resistance against the biotrophic fungal pathogen *G. cichoracearum* UCSC1 (Wang et al., 2011). We therefore performed resistance assays to compare the *G. cichoracearum* resistance of the *clc2-1 clc3-1* mutant, wild-type Col-0, and the *atg2-1* mutant. At 7 days post-inoculation (dpi), trypan blue staining was performed to monitor cell death, conidiophore production, and hyphal growth on the infected leaves. Cell death developed on the infected leaves of the *clc2-1 clc3-1* and *atg2-1* mutant plants but not on those of Col-0 (Figure 2D, see arrows). In addition, abundant fungal hyphae and conidiophores were visible on the leaves of the Col-0 plants, whereas many fewer hyphae and conidiophores were seen on the leaves of *clc2-1 clc3-1* and *atg2-1* plants (Figure 2E). To accurately quantify fungal reproduction, conidiophores were counted on the infected leaves at 7 dpi. As shown in Figure 2F, significantly fewer conidiophores formed on leaves of *clc2-1 clc3-1* mutant plants than on those of Col-0 plants, indicating that *G. cichoracearum* resistance was significantly enhanced in the *clc2-1 clc3-1* mutant.

clc2-1 clc3-1 mutant plants also displayed enhanced resistance against the biotrophic bacterial pathogen *Pst* DC3000 (Figure 1J and 1Q). However, the resistance of *atg* mutants to *Pst* DC3000 remains controversial (Hofius et al., 2009; Lenz et al., 2011; Wang et al., 2011). To resolve this issue, we performed bacterial growth assays. As shown in Figure 2G, growth of *Pst* DC3000 was significantly lower on leaves of both the *clc2-1 clc3-1* and *atg2-1* mutants than on those of Col-0 plants, indicating that the *clc2-1 clc3-1* and *atg2-1* mutants exhibited enhanced resistance against *Pst* DC3000. Together, our results indicate that the *clc2-1 clc3-1* and *atg2-1* mutants display similar resistance against two different types of biotrophic pathogen.

ATG2 is genetically epistatic to *CLC2/CLC3* in the carbon starvation response and in resistance to *G. cichoracearum*

To dissect the genetic relationship between *ATG2* and *CLC2/CLC3*, the *clc2-1 clc3-1 atg2-1* triple mutant was generated by crossing, and its response to dark treatment was compared with that of the *clc2-1 clc3-1* double-mutant and the *atg2-1* mutant. Both leaf chlorosis level and chlorophyl content of the triple mutant were reminiscent of those of the *atg2-1* mutant and more severe than those of the *clc2-1 clc3-1* double mutant (Figure 2H and 2I). We also compared the *G. cichoracearum*

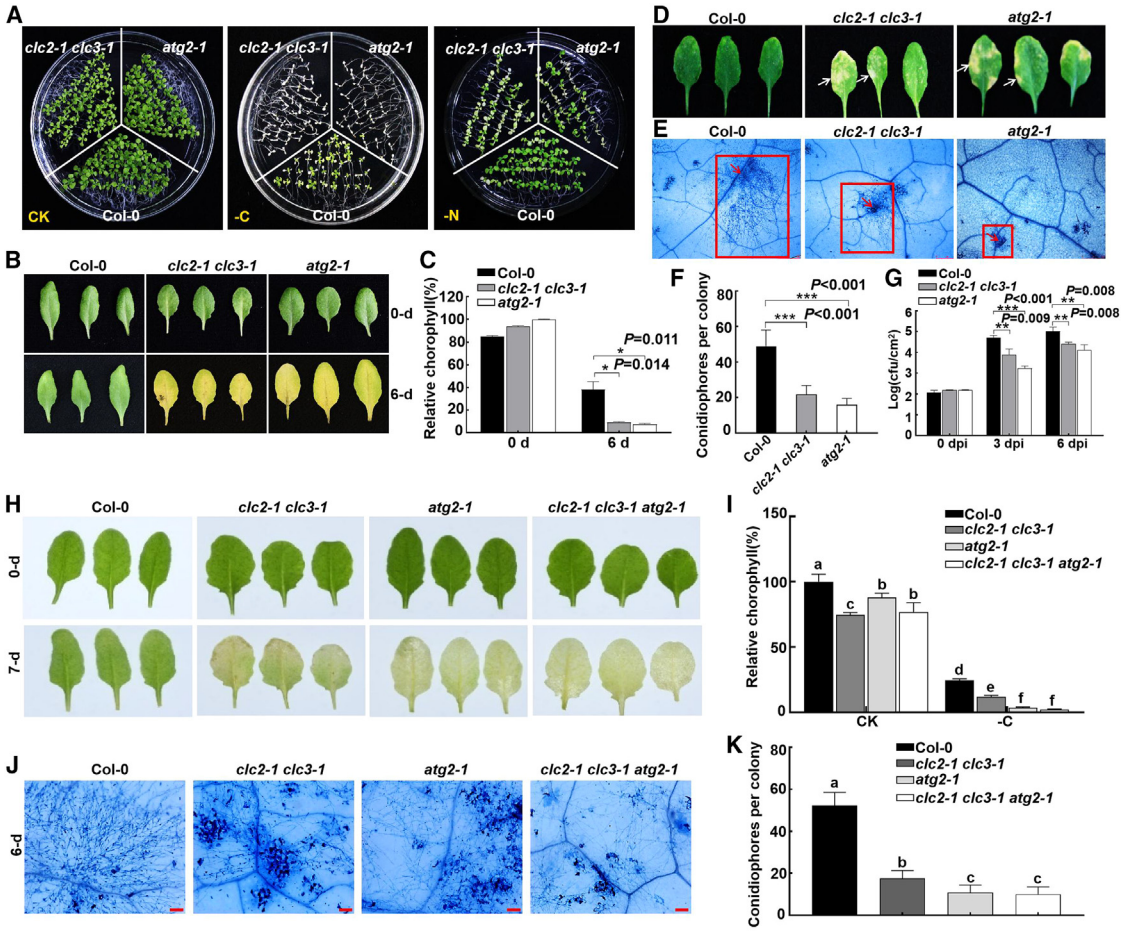

Figure 2. The *clc2-1 clc3-1* mutant phenocopies the *atg2-1* mutant in elevated nutrient sensitivity and enhanced immunity.

(A) Phenotype of the *clc2-1 clc3-1* double mutant under C and N starvation conditions (see details in materials and methods).

(B) Phenotype of dark-treated leaves from the equivalent positions of the indicated genotypes. Detached leaves from the 4-week-old plants were placed onto wet filter paper in petri dishes, which were wrapped with aluminum foil for dark treatment. Images were taken at 0 days (upper panel) and 6 days post dark treatment (lower panel).

(C) Relative chlorophyll contents of Col-0, *clc2-1 clc3-1*, and *atg2-1* seedlings. Asterisks indicate significant differences (*$p < 0.05$, two-tailed unpaired *t*-test). The experiments were repeated three times with similar results.

(D) Symptoms of 6-week-old Col-0, *clc2-1 clc3-1*, and *atg2-1* plants grown under short-day conditions (8-h light/16-h dark) infected with *G. cichoracearum.* The photos were taken at 7 dpi. The cell death caused by infection is indicated by arrows.

(E) Conidiophores and hyphal growth of *G. cichoracearum* on infected leaves were visualized by trypan blue staining. The boundaries of hyphae derived from a single colony are indicated by the red rectangles.

(F) Number of conidiophores formed on leaves of the different genotypes. Error bars represent the mean and standard deviation of one representative experiment. Asterisks indicate significant differences (***$p < 0.001$, two-tailed unpaired *t*-test, $n = 22$).

(G) *clc2-1 clc3-1* double-mutant and *atg2-1* mutant plants displayed enhanced resistance against *Pst* DC3000. cfu, colony-forming unit. Error bars represent the mean and standard deviation. Asterisks indicate significant differences (**$p < 0.01$; ***$p < 0.001$, two-tailed unpaired *t*-test, $n = 5$). The experiments were repeated three times with similar results.

(H) Phenotypes of detached rosette leaves from the indicated genotypes treated under dark conditions for 7 days. The detached leaves were placed upside down onto moist filter paper in petri dishes with the petioles wrapped in wet tissue paper. The photos were taken at 7 days post treatment. The experiment was repeated three times with similar results.

(I) Relative chlorophyll content of different genotypes after dark treatment. The chlorophyll content of Col-0 grown in 1/2 MS medium was set to 100%. Different letters indicate significant differences at $p < 0.001$ (one-way ANOVA with *post hoc* Duncan's test).

(J) Conidiophores and hyphal growth of *G. cichoracearum* on infected leaves of the indicated genotypes at 6 dpi were visualized by trypan blue staining.

(K) Number of conidiophores formed on leaves of the different genotypes. Error bars represent the mean and standard deviation of one representative experiment. Different letters indicate significant differences at $p < 0.001$ (one-way ANOVA with *post hoc* Duncan's test, $n > 15$).

resistance of the *clc2-1 clc3-1 atg2-1* triple mutant with that of the *clc2-1 clc3-1* double mutant and the *atg2-1* mutant. As shown in Figure 2J and 2K, the number of conidiophores on leaves of the *clc2-1 clc3-1 atg2-1* triple mutant was similar to that on leaves of the *atg2-1* mutant but significantly lower than that on leaves of the *clc2-1 clc3-1* double mutant. These results indicate that *ATG2* is genetically epistatic to *CLC2/CLC3*, both in the carbon starvation response and in resistance to *G. cichoracearum*.

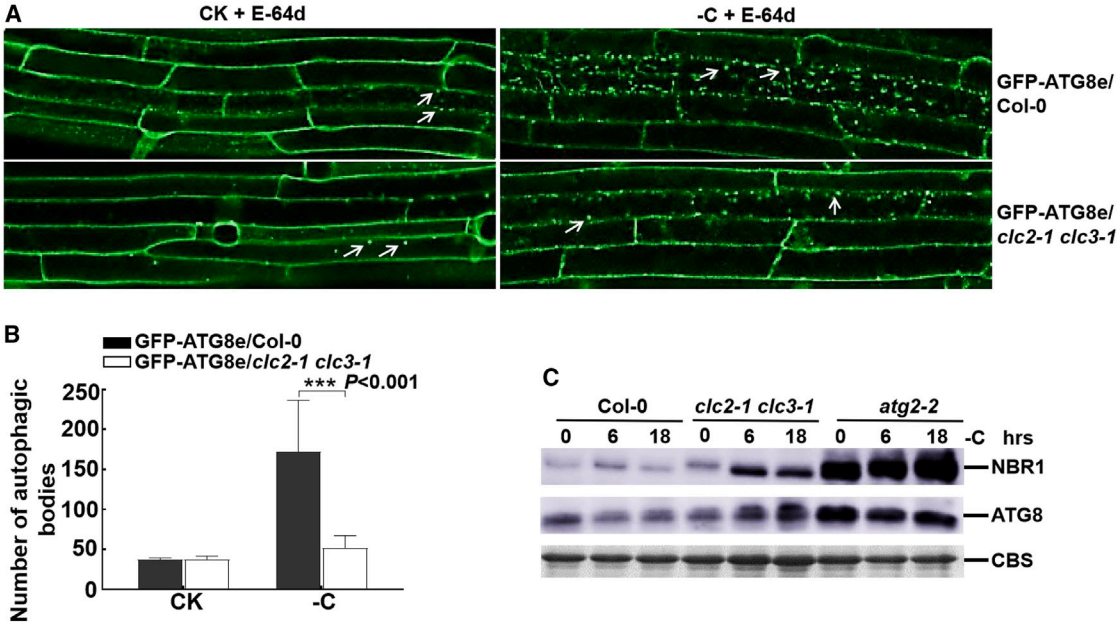

Figure 3. Autophagy is compromised in the *clc2-1 clc3-1* mutant.

(A) The number of autophagic bodies tagged by transgenically expressed GFP-ATG8e was significantly reduced in the *clc2-1 clc3-1* mutant seedlings. Five-day-old seedlings grown in 1/2 MS medium containing sucrose (CK, left panel) or no sucrose (−C, right panel) were treated with E64-d, a protease inhibitor, for 2 h. Primary root cells were observed, and images of the GFP-ATG8e bodies were captured by confocal microscopy.

(B) Quantification of the GFP-ATG8e bodies shown in **(A)**. Error bars represent the mean and standard deviation. Asterisks indicate significant differences (***$p < 0.001$, two-tailed unpaired *t*-test, $n > 15$).

(C) Autophagic degradation of both NBR1 (top panel) and ATG8 (middle panel) was attenuated in *clc2-1 clc3-1* mutant leaves. Coomassie blue staining (CBS) was used as a loading control (lower panel). Proteins were extracted from detached leaves of 4-week-old plants of the indicated genotypes that had been dark-treated for the indicated periods of time. Western blotting was performed using anti-*At*NBR1 or anti-*At*ATG8 antibody. The experiments were repeated three times with similar results.

Autophagy is compromised in *clc2-1 clc3-1* mutant plants

The similarities between the *clc2-1 clc3-1* and *atg2-1* mutant plants (Figure 2; Supplemental Figure 1) raised the possibility that autophagy is compromised in the *clc2-1 clc3-1* mutant. Various assays have been developed to monitor autophagy in plants (Li and Vierstra, 2012). Fusions of ATG8s with fluorescent proteins have been used as markers to visualize autophagosomes or autophagic bodies *in vivo* (Yoshimoto et al., 2004, 2009; Wang et al., 2011; Liu et al., 2020). In *Arabidopsis*, ATG8-labeled vesicles fail to accumulate in autophagy mutants (Yoshimoto et al., 2009; Chung et al., 2010). To test whether the *clc2-1 clc3-1* mutant exhibited autophagy defects, we examined the accumulation of autophagic bodies represented by GFP-ATG8e transgenically expressed in roots of 5-day-old Col-0 and *clc2-1 clc3-1* seedlings. Significantly fewer autophagic bodies were observed in root cells of the *clc2-1 clc3-1* mutant seedlings than in those of the Col-0 seedlings (Figure 3A and 3B), indicating that the autophagic pathway was compromised in the *clc2-1 clc3-1* mutant.

Accumulation of both ATG8s, which are structural components of autophagosomes, and NBR1, a selective receptor for ubiquitinated proteins, indicates a defect in the autophagy pathway (Yoshimoto et al., 2004). To confirm that the autophagy pathway was indeed impaired in the *clc2-1 clc3-1* mutant, we monitored the abundance of ATG8 and NBR1. As shown in Figure 3C, moderately increased accumulation of ATG8 and NBR1 was observed in *clc2-1 clc3-1* mutant plants relative to Col-0 plants under −C conditions, confirming that autophagic degradation was compromised in the *clc2-1 clc3-1* mutant. As a control, the *atg2-2* mutant showed substantially enhanced accumulation of both ATG8 and NBR1, even under CK conditions (Figure 3C). Accumulation of both ATG8 and NBR1 was higher in the *atg2-2* mutant than in the *clc2-1 clc3-1* mutant, regardless of C status (Figure 3C).

CLC2 but not CLC3 directly interacts with ATG8h and ATG8i

A CLC subunit was identified as an ATG8-interacting protein in *N. benthamiana* (Macharia et al., 2019), raising the possibility that CLCs might directly interact with ATG8s. To test this possibility, we performed yeast-two-hybrid (Y2H) assays of CLC2 or CLC3 with eight out of nine ATG8 variants (ATG8a–ATG8i, with the exception of ATG8b) in *Arabidopsis*. To our surprise, we found that AD-CLC2, but not AD-CLC3, specifically interacted with BD-ATG8h and BD-ATG8i (Figures 4A; Supplemental Figure 2), but not with other ATG8 isoforms (Figure 4A), suggesting that CLC2 participates in autophagy through direct interaction with ATG8h and ATG8i. Coincidentally, ATG8h and ATG8i are clustered into a closely related sub-clade (Supplemental Figure 3). The clade II isoforms (ATG8h and ATG8i) lack extra amino acid residues at the C terminus after the glycine residue, implying that ATG8h and ATG8i proteins can interact with the autophagosome membrane without ATG4 processing (Seo et al., 2016) (Supplemental Figure 4).

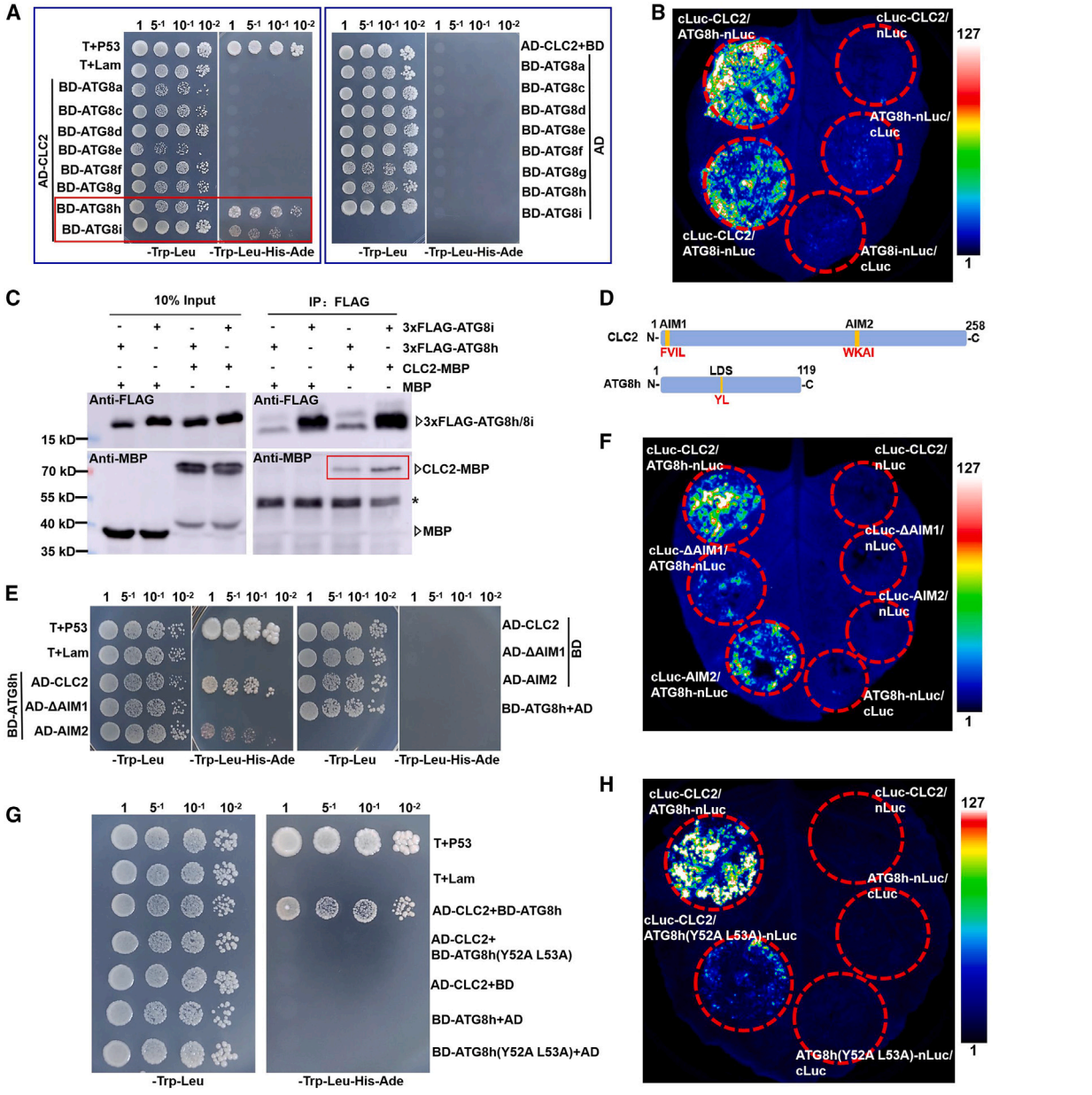

Figure 4. CLC2 interacts with ATG8h and ATG8i in an AIM1- and LDS-dependent manner.

(A) AD-CLC2 interacts specifically with BD-ATG8h and BD-ATG8i but not with the other ATG8s or the empty BD vector in Y2H assays. Yeast cells on the left were selected on SD/Trp-Leu medium, and yeast cells on the right were selected on SD/Trp-Leu-His-Ade medium.

(B) cLuc-CLC2 interacts with ATG8h-nLuc and ATG8i-nLuc in a luciferase complementation assay.

(C) Co-immunoprecipitation of CLC2-MBP and 3xFLAG-ATG8h/3xFLAG-ATG8i after co-expression in leaves of *N. benthamiana* via agro-infiltration. At 2 d post infiltration, protein extracts of infiltrated leaf tissues were incubated with agarose beads coated with FLAG antibody. Western blotting was performed using anti-FLAG or anti-MBP antibody. Molecular weight (kDa) marker bands are indicated. * represents the band that cross-reacted with the IgG heavy chain of the secondary antibody according to the manufacturer's manual.

(D) Diagrams showing the locations of the AIMs and LDS in CLC2 and ATG8h, respectively.

(E) The interaction between CLC2 and ATG8h was abolished by AIM1 deletion (ΔAIM1) but not by AIM2 mutations in a Y2H assay.

(F) The luminescence reflecting the interaction between cLuc-CLC2 and ATG8h-nLuc was abolished by AIM1 deletion (ΔAIM1) but not by AIM2 mutations.

(G) The interaction between CLC2 and ATG8h was abolished by LDS mutations at Y52A and R53A within ATG8h in a Y2H assay.

(H) The interaction between CLC2 and ATG8h was abolished by LDS mutations at Y52A and R53A within ATG8h in a luciferase complementation assay. T-antigen and p53 were included as a positive interaction control, and Lam and T-antigen were included as a negative interaction control in **(A)**, **(E)**, and **(G)**. The photos in **(A)**, **(E)**, and **(G)** were taken at 4 days post incubation. AD, activation domain; BD, binding domain. The numbers on top of the images are the dilution factors. In **(F)** and **(H)**, the luciferase complementation assay was performed by agro-infiltration of the indicated pairs of constructs into *N. benthamiana* leaves. The images were captured by a CCD imaging system at 2 days post infiltration. These experiments were repeated three times with similar results.

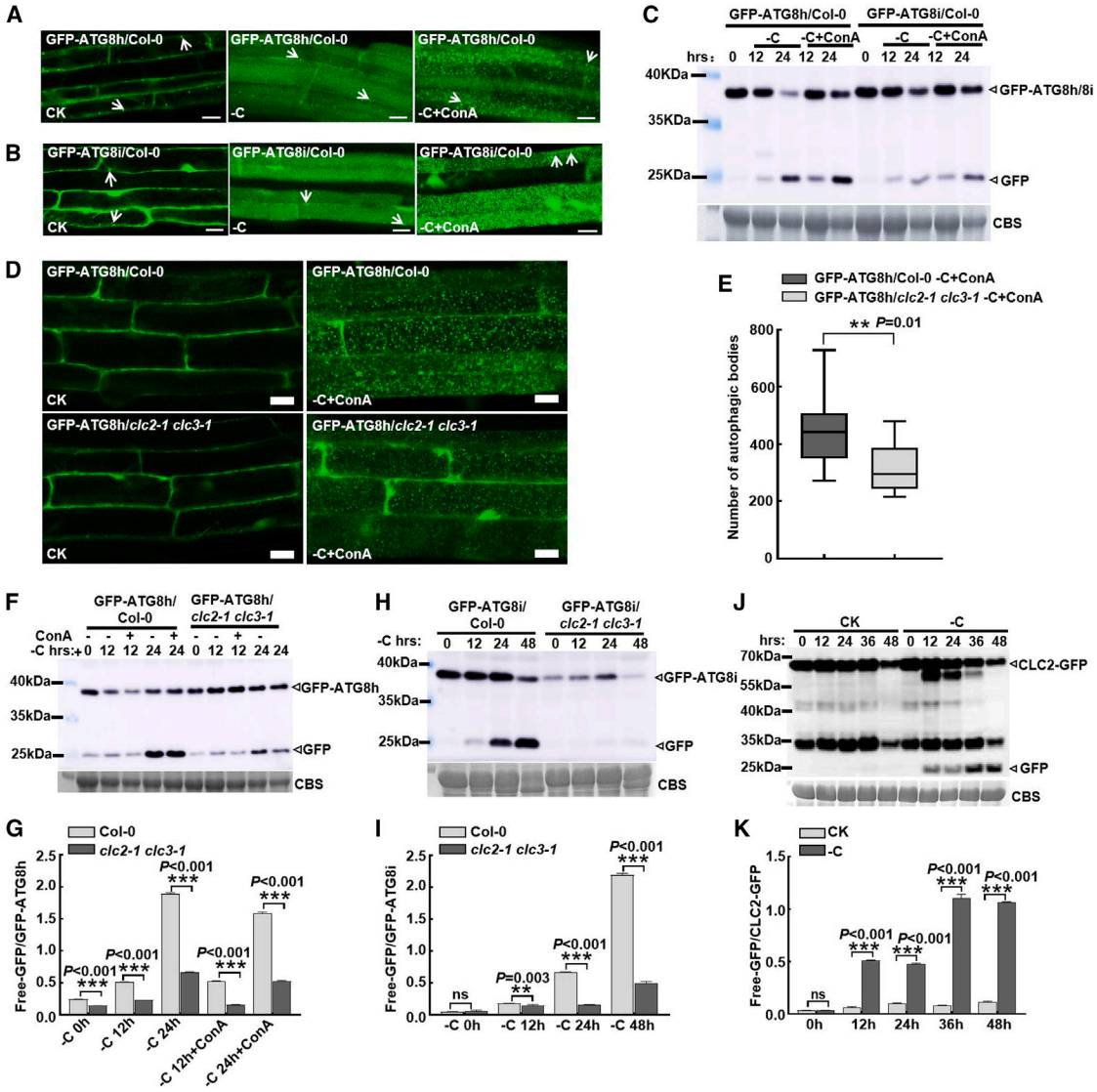

Figure 5. GFP-ATG8h and GFP-ATG8i are subjected to autophagic degradation, and the autophagic flux of GFP-ATG8h is significantly reduced in the *clc2-1 clc3-1* mutant.

(A and B) Seven-day-old Col-0 seedlings expressing GFP-ATG8h or GFP-ATG8i were grown under CK conditions for 48 h (upper panel), under −C conditions for 48 h (middle panel), or under −C conditions for 36 h followed by addition of 1 μM ConA for 12 h (lower panel). GFP signals in the root cells were visualized by laser confocal microscopy. White arrows point to autophagosomes or autophagic bodies. Bars, 20 μm.

(C) Free GFP was released from GFP-ATG8h and GFP-ATG8i under autophagy-inducing conditions. Seven-day-old GFP-ATG8h/WT and GFP-ATG8i/WT seedlings were grown in −C liquid medium with or without 1 μM ConA for 12 h and 24 h. The free GFP released from GFP-ATG8h or GFP-ATG8i as a result of autophagic degradation was detected by western blotting with GFP antibody. CBS was used as a loading control.

(D) Formation of autophagic bodies of GFP-ATG8h induced by dark treatment in the presence of ConA was significantly reduced in the *clc2-1 clc3-1* root cells relative to those of Col-0 (right panel). Bars, 20 μm.

(E) Comparison of the number of autophagic bodies induced by −C+ConA treatment in the same area of the root cells in Col-0 and *clc2-1 clc3-1* as shown in **(D)** (right panel). Autophagic bodies were counted using ImageJ software. Asterisks indicate significant differences (**$p < 0.01$, two-tailed unpaired *t*-test, $n > 11$). The error bars represent the ranges of the number of autophagic bodies. The bars inside the columns represent the average number of autophagic bodies.

(F) Release of free GFP from GFP-ATG8h is significantly reduced in the *clc2-1 clc3-1* double mutant. Seven-day-old *35S::GFP-ATG8h*/WT and *35S::GFP-ATG8h/clc2-1 clc3-1* seedlings were grown in −C liquid medium with or without 1 μM ConA for 12 h or 24 h. Total protein was extracted from the seedlings, and the free GFP released from GFP-ATG8h was detected by western blotting with anti-GFP antibody as an indicator of autophagic degradation. CBS was used as a loading control.

(G) Free GFP/GFP-ATG8h ratios calculated from the band intensities shown in **(F)**.

(H) Release of free GFP from GFP-ATG8i is significantly reduced in the *clc2-1 clc3-1* double mutant. Seven-day-old *35S::GFP-ATG8i*/WT and *35S::GFP-ATG8i/clc2-1 clc3-1* seedlings were grown in −C liquid medium for 12, 24, and 48 h.

(I) Free GFP/GFP-ATG8i ratios calculated from the band intensities shown in **(H)**.

(legend continued on next page)

The CLC2–ATG8h/ATG8i interactions were confirmed by both a luciferase complementation assay (Figure 4B) and a co-immunoprecipitation (Co-IP) assay (Figure 4C). These results demonstrate that CLC2 indeed interacts with ATG8h and ATG8i.

CLC2 interacts with ATG8h through a unique AIM present in CLC2 and the LDS present in ATG8h

It has been established that cargo receptors interact with ATG8 proteins anchored on the autophagosome membrane through the AIM for cargo recruitment (Noda et al., 2010). Two putative AIMs were identified in the amino acid sequence of CLC2 and CLC3 (Figures 4D; Supplemental Figure 5). In addition to a common AIM shared by CLC2 and CLC3, both CLC2 and CLC3 also have a unique AIM (Supplemental Figure 5). The fact that CLC3 did not interact with ATG8h/8i (Supplemental Figure 2) strongly suggests that the CLC2–ATG8h/8i interaction is most likely mediated by the AIM1 that is unique to CLC2 near its N terminus (Figure 4D, upper panel; Supplemental Figure 5). To explore this possibility, an AIM1 deletion version (ΔAIM1) of CLC2 and a version with the first and fourth amino acids of AIM2 (WKAI) mutated to Ala (**A**KA**A**) were generated by site-directed mutagenesis and tested for interaction with ATG8h using Y2H and luciferase complementation assays. Consistent with our hypothesis, only the AIM1 deletion, but not the AIM2 mutations, abolished the CLC2–ATG8h interaction (Figure 4E and 4F), indicating that CLC2 interacts with ATG8h in an AIM1-dependent manner.

The LDS present in the ATG8 protein family is critical for interactions between ATG8 proteins and autophagic receptors/adaptors, which lead to the recruitment of cargoes to autophagosomes. A hydrophobic pocket is highly conserved in the LDS of the ATG8 isoforms (Yamaguchi et al., 2010; Marshall et al., 2019) (Figure 4D, lower panel; Supplemental Figure 4). Simultaneous mutations of Y50 and L51 in the hydrophobic pocket to Alanine (A) (Y50A, L51A) abolished the LDS binding affinity of ATG8a or ATG8f (Marshall et al., 2019). Therefore, we generated the Y52A/L53A mutant of ATG8h by site-directed mutagenesis. Consistent with previous reports, Y52A/L53A substitutions in ATG8h significantly weakened its interaction with CLC2 in both Y2H (Figure 4G) and luciferase complementation assays (Figure 4H). Together, these results indicate that both the AIM1 in CLC2 and the LDS in ATG8h are essential for the CLC2–ATG8h interaction.

Both GFP-ATG8h and GFP-ATG8i are subjected to autophagic degradation

ATG8 proteins decorate the membranes of autophagosomes usually destined for the vacuoles for autophagic degradation. To test whether ATG8h and ATG8i similarly enter vacuoles and are subjected to autophagic degradation, we generated *35S::GFP-ATG8h* and *35S::GFP-ATG8i* transgenic seedlings. We then examined the effects of dark treatment as well as dark + ConA, an inhibitor of autophagic degradation, on the degradation of autophagic bodies labeled by GFP in root cells. Under long-day conditions (16-h light/8-h dark), only a few autophagic bodies labeled by GFP-ATG8h or GFP-ATG8i were observed (Figure 5A and 5B, upper panels, see white arrows). Under autophagy-inducing conditions (constant dark treatment for 48 h), diffuse fluorescence was observed in root cells of both the *35S::GFP-ATG8h* and *35S::GFP-ATG8i* seedlings (Figure 5A and 5B, middle panels), indicating that the autophagic bodies labeled by GFP-ATG8h or GFP-ATG8i were mostly degraded into free GFP inside the vacuoles. However, numerous autophagic bodies labeled by GFP-ATG8h or GFP-ATG8i were observed upon dark treatment followed by ConA treatment owing to inhibition of autophagic degradation (Figure 5A and 5B, lower panels, see white arrows). These results demonstrate that, like other ATG8 proteins, GFP-ATG8h and GFP-ATG8i enter the vacuoles and are subjected to autophagic degradation.

The release of free GFP from GFP-ATG8 fusion proteins during breakdown of the autophagic bodies can be used to measure autophagy-dependent vacuolar transport and degradation (Yoshimoto et al., 2004; Chung et al., 2010). To further examine whether GFP-ATG8h and GFP-ATG8i are similarly subject to autophagic degradation, *35S::GFP-ATG8h*/*35S::GFP-ATG8i* transgenic seedlings were treated in the dark in C-deficient 1/2 MS medium to mimic C deprivation and thus induce autophagy. As shown in Figure 5C, the C-starvation treatment significantly increased the release of free GFP from both GFP-ATG8h and GFP-ATG8i. Treatment with ConA increased the levels of undegraded GFP-ATG8h and GFP-ATG8i, indicating that GFP-ATG8h and GFP-ATG8i are degraded in the vacuoles via the autophagy pathway.

Autophagic degradation of GFP-ATG8h/GFP-ATG8i is significantly reduced in the *clc2-1 clc3-1* double mutant

Because autophagy was impaired in the *clc2-1 clc3-1* double mutant (Figure 3) and CLC2 interacted with ATG8h (Figure 4), we reasoned that the autophagic degradation of GFP-ATG8h would be reduced in the *clc2-1 clc3-1* double mutant. To test this possibility, *35S::GFP-ATG8h* was crossed into the *clc2-1 clc3-1* background, and the formation of autophagic bodies induced by dark treatment in the presence of ConA was compared between Col-0 and *clc2-1 clc3-1* seedlings. As expected, formation of autophagic bodies was significantly reduced in the *clc2-1 clc3-1* seedlings relative to the Col-0 seedlings (Figure 5D and 5E), indicating that loss of CLC2/CLC3 function compromises the autophagic flux but does not abolish it. Release of free GFP from GFP-ATG8h or GFP-ATG8i as a result of autophagic degradation was also significantly reduced in *clc2-1 clc3-1* seedlings relative to Col-0 seedlings (Figure 5F–5I). Collectively, these results indicate that loss of CLC2/CLC3 function significantly reduces autophagic flux and confirm the functional relevance of the CLC2–ATG8h/ATG8i interactions.

(J) Free GFP was released from CLC2-GFP under autophagy-inducing conditions. *Agrobacterium* strain GV3101 carrying the *35S::CLC2-GFP* construct was infiltrated into leaves of *N. benthamiana*. At 1.5 days post infiltration, the infiltrated leaves were kept in the light or in the dark for the indicated hours. The free GFP released from CLC2-GFP was detected by western blotting with anti-GFP antibody. CBS was used as a loading control.
(K) The free GFP/CLC2-GFP ratio calculated from the band intensities shown in **(H)**. The intensity of each band shown in **(F)** and **(H)** was quantified using ImageJ software. Asterisks indicate significant differences (**$p < 0.01$; ***$p < 0.001$, two-tailed unpaired *t*-test).

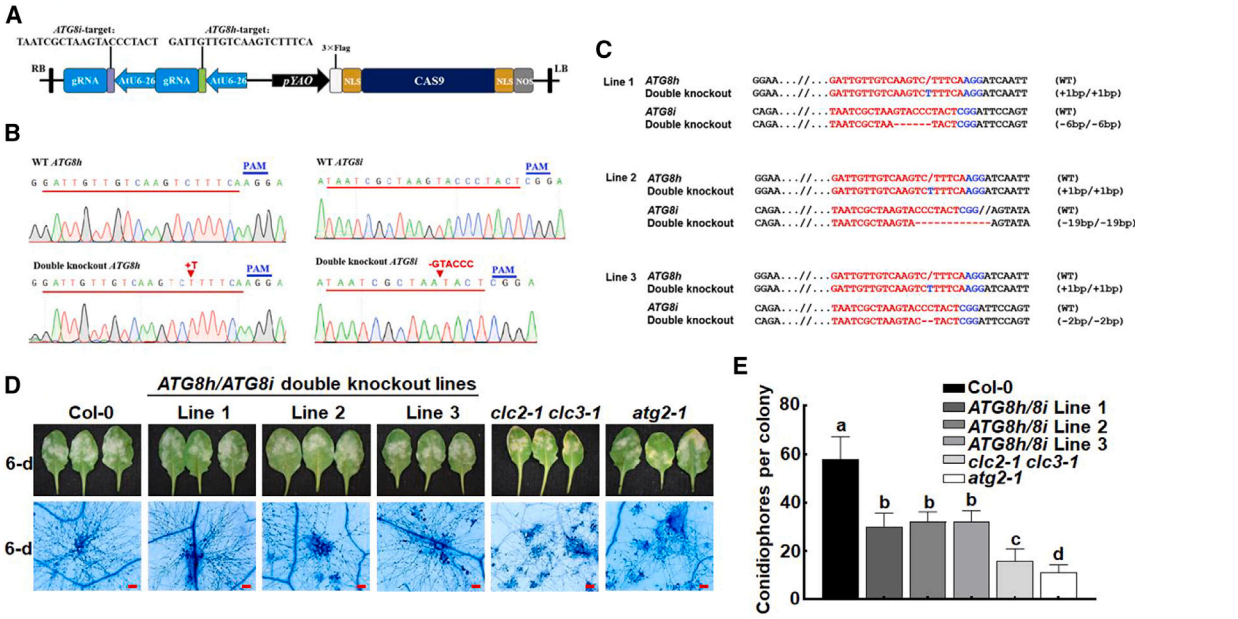

Figure 6. Simultaneous knockout of *ATG8h* and *ATG8i* results in enhanced resistance against *G. cichoracearum*.

(A) Diagram of the CRISPR-Cas9 dual-target construct used to generate transgenic plants with knockout of both *ATG8h* and *ATG8i*.

(B) Sequencing chromatograms near the edited regions of the WT and CRISPR-Cas9 knockout line 1, in which both *ATG8h* and *ATG8i* are edited simultaneously. Arrows point to the sites of insertions or deletions. + represents insertion and − represents deletion. The PAM sequences are marked in blue.

(C) Sequence alignments of three CRISPR-Cas9 double-knockout lines at the *ATG8h* and *ATG8i* loci. The short red horizontal lines represent the deletions; the blue A/CGG represents the PAM sequence; and the blue letters represent the insertions; "/" represents an extra space added for the purpose of perfect sequence alignment. The mutation types of the CRISPR-Cas9 line are presented by the labeling on the right.

(D) Symptoms, conidiophores, and hyphal growth of *G. cichoracearum* on infected leaves of the indicated genotypes. Photos of fungal symptoms on infected leaves were taken at 6 dpi (upper panel), and photos of conidiophores and hyphal growth were taken under a microscope at 6 dpi.

(E) Number of conidiophores formed on the leaves of different genotypes. Bars represent the mean and standard deviation of one representative experiment. Different letters indicate significant differences among genotypes. $p < 0.001$ (one-way ANOVA with *post hoc* Duncan's test, $n > 15$). The experiments were repeated five times with similar results.

CLC2-GFP is subjected to autophagic degradation

To test the possibility that CLC2–ATG8h/ATG8i interactions mediate autophagic degradation of CLCs, the *35S::CLC2-GFP* construct was transiently expressed in leaves of *N. benthamiana* by agro-infiltration, and release of free GFP from the expressed CLC2-GFP was examined. Under normal growth conditions, release of free GFP was barely detectable (Figure 5J). However, release of free GFP was significantly induced by C starvation (Figure 5J and 5K), indicating that CLC2-GFP was subjected to autophagic degradation under these conditions. Collectively, these data indicate that both GFP-ATG8h/GFP-ATG8i and CLC2-GFP are targeted to the vacuoles for autophagic degradation and that the autophagic degradation of CLC2 is most likely mediated by interaction with ATG8h/ATG8i (Figure 4).

Simultaneous knockout of *ATG8h* and *ATG8i* by CRISPR-CAS9 enhances resistance against *G. cichoracearum*

To further investigate the functional relevance of the CLC2–ATG8h/ATG8i interactions, we generated CRISPR-CAS9 lines in which both *ATG8h* and *ATG8i* were simultaneously knocked out by a dual-target CRISPR-CAS9 construct (Figure 6A). Sequencing of the T3 populations confirmed that both *ATG8h* and *ATG8i* were knocked out in three independent lines (Figure 6B and 6C). Under normal growth conditions, no discernible phenotype was observed for these lines. However, as observed in the *atg2-1* and *clc2-1 clc3-1* mutants, the resistance of these double knockout lines against *G. cichoracearum* was significantly enhanced relative to that of Col-0 (Figure 6D and 6E). Collectively, these results indicate that the CLC2–ATG8h/ATG8i interactions are functionally relevant in the context of resistance against *G. cichoracearum*.

The enhanced resistance of the *ATG8h/ATG8i* knockout lines and the *atg2-1* and *clc2-1 clc3-1* mutant plants to *G. cichoracearum* (Figure 6D and 6E) indicated an enhancement of immunity in these mutant lines. To investigate the basis of this enhanced resistance, we compared callose deposition and *PR1* gene induction in response to flg22 treatment. As shown in Supplemental Figure 6, both callose deposition and *PR1* expression were significantly induced in the mutant lines compared with wild-type Col-0, indicating that increased callose deposition and *PR1* induction are responsible for the enhanced resistance observed in these mutants. These results also indicate that the *clc2-1 clc3-1* mutant phenocopies the *ATG8h/ATG8i* double mutants in immune responses.

ATG8h/ATG8i knockout accelerates cell death induced by the fungal toxin fumonisin B1

We next examined the effect of *ATG8h/ATG8i* knockout on the cell death induced by fumonisin B1 (FB1), a fungal toxin secreted

from the necrotrophic pathogen *Fusarium moniliforme*, which can mimic fungal-induced cell death (Wang et al., 1996; Gilchrist, 1997). To this end, 10 μM FB1 was infiltrated into leaves of Col-0, the *atg8hatg8i* double knockout lines, the *atg2* mutant, and the *clc2-1 clc3-1* mutant. As shown in Supplemental Figure 7, although cell death was clearly observed on leaves of the *agt8hatg8i*, *atg2*, and *clc2-1 clc3-1* plants at 4 and 5 days post infiltration, no apparent cell death was induced on leaves of Col-0 plants (Supplemental Figure 7), suggesting that ATG8h/ATG8i play a role in restricting the cell death induced by FB1. In this regard, the *clc2-1 clc3-1* double-mutant phenocopies the *ATG8h/8i* double-knockout lines and *atg2-1* mutant. Taken together, our results suggest that autophagy plays a negative role in immunity but an anti-death role in restricting cell death induced by the necrotrophic toxin FB1.

DISCUSSION

Our findings provide direct genetic, biochemical, and cytological evidence of a direct link between the function of CLCs and the autophagy pathway.

Functions of *Arabidopsis* CLC2 and CLC3 in SA- and H_2O_2-dependent cell death and their relationship with autophagy

The similarities between the *clc2-1 clc3-1* and *atg* mutants in SA- and H_2O_2-dependent accelerated senescence, activated defense responses, and enhanced resistance to biotrophic pathogens (Figures 1 and 2) strongly indicate a close interconnection between CLC2/CLC3 functions and the autophagy pathway. Mutations in many *ATG* genes result in over-accumulation of SA and H_2O_2, accelerated senescence, and excessive programmed cell death (PCD), irrespective of nutrient conditions (Hanaoka et al., 2002; Yoshimoto et al., 2009; Chung et al., 2010; Wang et al., 2011). Accelerated senescence and PCD are suppressed by SA degradation, impairment of SA biosynthesis, or blocking of SA signaling (Yoshimoto et al., 2009; Wang et al., 2011). These results indicate that autophagy negatively regulates SA homeostasis and signaling and that this negative feedback mechanism keeps senescence and immunity-related PCD under control (Yoshimoto et al., 2009). Given that loss of CLC2 and CLC3 compromises the autophagy pathway in *Arabidopsis* (Figure 3), the autoimmune phenotypes observed in the *clc2-1 clc3-1* mutant (Figure 1) most likely originate from compromised autophagy.

The autoimmune phenotypes of the *clc2-1 clc3-1* mutant were not only rescued by loss of function of SID2/ICS1 but also by loss of function of RBOHD (Figure 1K–1Q). These findings strongly indicate that both RBOHD-dependent H_2O_2 and SID2/ICS1-dependent SA are absolutely required for triggering of autoimmune responses in the *clc2-1 clc3-1* mutant plants and that the presence of either elevated SA or H_2O_2 alone is not sufficient to initiate and/or maintain the positive SA–ROS amplification loop (Figure 1K–1Q). In support of this conclusion, it has been shown that increased ROS levels induce SA biosynthesis (Neuenschwander et al., 1995) and that SA induces strong oxidative stress responses (Rao et al., 1999). The over-accumulation of ROS in the *atg2* and *atg5* mutant plants was significantly reduced in*NahG* and *sid2* backgrounds (Yoshimoto et al., 2009). Our findings suggest that CLC2/CLC3 function is required for attenuation of the SA–ROS feedback amplification loop (Figure 1), which may be executed through the autophagy pathway.

Potential roles of clathrin in autophagy

Numbers of autophagosomes and/or autophagic bodies were significantly reduced in the *clc2-1 clc3-1* mutant in the presence of E-64d, a Cys protease inhibitor that blocks protein degradation in the vacuole (Figure 3A and 3B). This could be due to impaired formation of autophagosomes, reduced delivery of autophagosomes into vacuoles, compromised degradation of autophagic bodies inside vacuoles, or any combination of these possibilities (Zhuang et al., 2015). The fact that C-starvation-induced accumulation of ATG8 and NBR1 was not increased in leaves of the *clc2-1 clc3-1* mutant to the extent observed in the *atg2-2* mutant in the presence of E-64d (Figure 3C) suggests that, in addition to degradation in the vacuoles, biogenesis of autophagosomes is likely compromised in *clc2-1 clc3-1*. In other words, the function of CLC2/CLC3 is required for autophagosome formation. A functional connection between clathrin and autophagy has previously been reported in mammals. In human cells, autophagy contributed to connexin 31.1 (Cx31.1) degradation, and clathrin may be involved in the autophagy of Cx31.1 (Zhu et al., 2015). Clathrin, AP2, AP4, and PtdIns(4,5)P2 directly mediate budding of the autolysosome in rats (Rong et al., 2012). The human clathrin adaptor protein AP1 and clathrin were localized to starvation- and rapamycin-induced autophagosomes, and dysfunction of the AP1-dependent clathrin coating at the TGN prevented autophagosome formation (Guo et al., 2012). In mammalian cells, CHC and AP-2 interact with Atg16L1, and depletion of CHC and AP-2 moderately but significantly reduces autophagy initiation and the formation of pre-autophagosome structures (Ravikumar et al., 2010; Lamb et al., 2012). A recent quantitative proteomics study revealed that clathrin heavy and light chains, PIK3C2A (a phosphoinositide 3-kinase involved in clathrin-mediated endocytosis), and several clathrin adaptors associate with ATG5. Knockout of any of these proteins alters autophagic flux under starvation conditions. These results link clathrin-mediated vesicular trafficking with the autophagosome assembly machinery (Baines et al., 2022).

Although indirect evidence implies that clathrin may play a role in plant autophagy, direct evidence that clathrin plays a role in autophagy is still lacking. SH3-DOMAIN CONTAINING PROTEIN 2 (SH3P2), a BAR (Bin-Amphiphysin-Rvs) domain protein, was shown to participate in autophagosome formation in *Arabidopsis* by interacting with ATG8e/8f and PI3P and associating with PI3K (Zhuang et al., 2013). SH3P2 localizes to the PM, associates with CCVs, co-localizes with CLC-labeled structures, and coimmunoprecipitates with CHC (Nagel et al., 2017). On the basis of these observations, clathrin is proposed to play a role in the initiation of autophagosome formation, membrane expansion, or maturation or cargo sorting in *Arabidopsis* (Zhuang et al., 2013, 2015). *Arabidopsis* AtEH1/Pan1 and AtEH2/Pan1 proteins, the subunits of the endocytic TPLATE complex (TPC), are involved in actin-cytoskeleton-regulated autophagy (Wang et al., 2019). When autophagy is induced, AtEH/Pan1 proteins recruit TPC and AP-2 subunits, CHC, and ARP2/3 proteins for the formation of autophagosomes through interaction with F-actin and VAMP-ASSOCIATED-PROTEIN 27-1 (VAP27-1) at ER (endoplasmic reticulum)–PM contact sites (Wang et al., 2019). However,

comparison of mutants in the CME pathway with *atg* mutants was not included in these studies. Therefore, it is unclear whether these mutants share similar morphological phenotypes and biochemical characteristics with *atg* mutants. In addition, direct genetic evidence for the involvement of CLCs or CHCs in SH3P2- or AtEH/Pan1-mediated autophagy was not provided (Zhuang et al., 2013, 2015; Wang et al., 2019).

Functional relevance of the CLC2–ATG8h/ATG8i interactions

The unique feature of the ATG8h/8i group is that they have an exposed catalytic glycine residue at the C terminus (Figure 5S) and do not require cleavage by the ATG4 protease for activation (Seo et al., 2016; Kellner et al., 2017), suggesting that they may have an advantage over other ATG8s in swiftly responding to nutrient deprivation or other stress conditions. The cargoes targeted by selective autophagy are usually recognized by cargo receptors that interact with membrane-anchored ATG8s through the AIM present on the cargo receptors (Noda et al., 2010; Birgisdottir et al., 2013). ATG8h has been reported to interact with ATG8-INTERACTING PROTEIN 1 (ATI1) localized to ER/plastid bodies (Avin-Wittenberg et al., 2012). These interactions function to target the damaged ER/plastid and/or ER/plastid proteins to the vacuoles for degradation (Michaeli et al., 2014). Therefore, it is plausible that CLC2–ATG8h/ATG8i–ATI1/2 interactions redirect the ER/plastid bodies to sites of autophagosome formation for the membrane components. Tomato ATG8h interacts with AVRPTO-DEPENDENT PTO-INTERACTING PROTEIN 3 (Adi3), an AGC protein kinase that functions to suppress PCD (Devarenne, 2011). In another case, the interaction of nucleus-localized C1, a replication initiator protein of Tomato leaf curl Yuannan virus (TLCYnY), with NbATG8h leads to translocation of C1 protein from the nucleus to the cytoplasm and results in its degradation by selective autophagy in an AIM-dependent manner (Li et al., 2019).

We showed that CLC2 interacts with ATG8h/ATG8i in an AIM1- and LDS-dependent manner (Figure 4). The functional relevance of the CLC2–ATG8h/ATG8i interaction was reflected by the fact that free GFP release from GFP-ATG8h was significantly reduced in *clc2-1 clc3-1* seedlings relative to Col-0 seedlings (Figures 5F and 5G). In addition, simultaneous knockout of *ATG8h* and *ATG8i* enhanced resistance against *G. cichoracearum* (Figure 6). These results suggest that CLC2 may serve as an autophagic receptor to selectively mediate the autophagic degradation of CLC2 itself (Figures 5H and 5I) and CCVs, including EEs/TGNs, which are coated with clathrins (Viotti et al., 2010), and that this may in turn regulate the progression of autophagy (Zhuang et al., 2015). However, the CLC2–ATG8h/ATG8i interactions may also provide a means to deliver CCVs carrying lipids/phospholipids (lipid nanodrops), proteins, or other necessary components derived from PM or PM–ER contact sites to sites of autophagosome biogenesis (Zhuang et al., 2013, 2015; Gomez et al., 2022). This statement is supported by the significantly reduced autophagic flux observed in the root cells of *clc2-1 clc3-1* mutant seedlings under C-starvation conditions (Figures 3A–3C; 5D–5G) and the C-starvation-induced GFP release from CLC2-GFP resulting from autophagic degradation (Figure 5H and 5I). The fact that the formation of C-starvation-induced autophagic bodies visualized by GFP-ATG8e was also significantly reduced (Figure 3A and 3B) and that both ATG8s and NBR1 were over-accumulated in the *clc2-1 clc3-1* mutant (Figure 3C) indicated that loss of CLC2 and CLC3 function impairs overall autophagy, not just ATG8h/ATG8i-mediated autophagy. Given that clathrin is also involved in post-Golgi trafficking (Yan et al., 2021), CLC2–ATG8h/ATG8i interactions may provide membrane components or proteins required for the biogenesis of autophagosomes from the ER or ER–PM contact sites through the secretory pathway (Ravikumar et al., 2010; Zhuang et al., 2013; 2015).

On the basis of data reported here, together with previously published results, we propose a model to explain the importance of CLC2–ATG8h/ATG8i interactions in *Arabidopsis* immunity. As discussed earlier, ATG8h/ATG8i may guide the CCVs to deliver their cargoes—such as lipids, proteins, or other required components—to sites of autophagosomal initiation, expansion, or enclosure through direct interaction with CLC2 (Figure 4). Plants constantly encounter numerous biotic/abiotic stresses, even under normal growth conditions, which lead to production of RBOHD-dependent ROS (referred to as primary ROS) as a result of activation of PTI or stress responses. Primary ROS usually induce SA biosynthesis and initiate the ROS–SA amplification loop (Guo et al., 2017). As a result, organelles such as chloroplasts, mitochondria, and peroxisomes are damaged by severe oxidation. Oxidized chloroplasts, mitochondria, and peroxisomes are the major sources of organelle-derived ROS (referred to as secondary ROS). In Col-0, severely oxidized organelles are effectively cleared by forms of autophagy, such as chlorophagy, mitophagy, and perophagy (Ran et al., 2020), thus quenching secondary ROS production and resulting in regulated immunity (Figure 7, left panel). However, in the *clc2-1 clc3-1* mutant, CLC2–ATG8h/ATG8i interactions no longer take place, and autophagosome biogenesis, which requires the coordinated action of most ATG proteins including ATG2, is therefore compromised. As a result, oxidized organelles cannot be effectively cleared through the autophagy pathway and over-accumulate in the cytoplasm, resulting in a burst of secondary ROS production. ROS over-accumulation constitutively activates immunity and ultimately induces cell death (Figure 7, right panel).

Right after our findings were posted in bioRxiv (Lan et al., 2023), Zhou et al. (2023) reported that CLC2 was recruited to the cistern membrane of the Golgi by interaction with ATG8s to facilitate Golgi reassembly under heat stress. The authors identified CLC2 as an interaction partner of ATG8a using TurboID-based proximity labeling, followed by verification using Y2H and BiFC assays (Zhou et al., 2023). They subsequently showed in a Y2H assay that CLC2 interacted not only with ATG8a but also with eight other members of the ATG8 protein family. They also showed that ATG8e interacted with CLC2 in an AIM- and LSD-dependent manner in both Y2H and BiFC assays. However, our results demonstrated that CLC2 only interacted specifically with ATG8h and ATG8i and not with the rest of the ATG8 isoforms (Figure 4). The reason for this apparent discrepancy remains to be addressed in the future.

MATERIALS AND METHODS

Materials

The *atg2-1* (SALK_076727) (Yoshimoto et al., 2009) and *atg2-2* (Wang et al., 2011) T-DNA mutants were obtained from

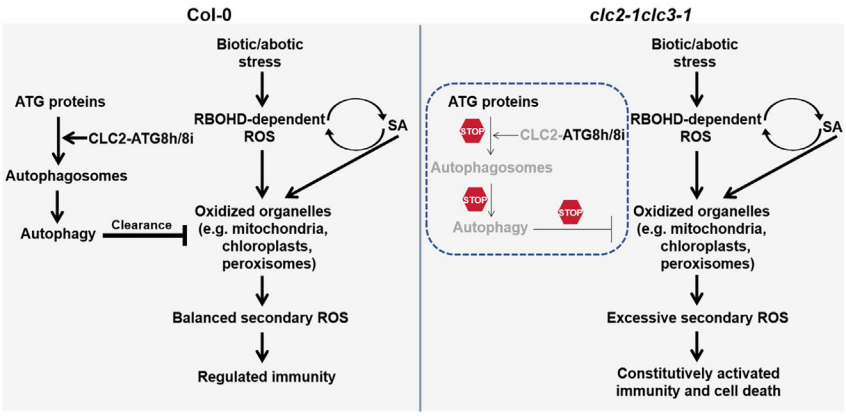

Figure 7. A proposed working model illustrating the roles of CLC2–ATG8h/ATG8i interactions in regulation of *Arabidopsis* immunity.

Plants constantly encounter numerous biotic/abiotic stresses, even under normal growth conditions, which lead to production of RBOHD-dependent ROS (referred to as primary ROS) as a result of activation of immunity or stress responses. In WT Col-0, CLC2–ATG8h/ATG8i interactions facilitate delivery of the cargoes of clathrin-coated vesicles (CCVs), such as lipids and/or proteins that are required for the biogenesis of autophagosomes, which are in turn required for autophagic clearance of oxidized organelles such as mitochondria, chloroplasts, and peroxisomes, the major sources of secondary ROS. Clearance of the oxidized organelles keeps secondary ROS production in check and thus results in a regulated immunity (left). In the *clc2-1 clc3-1* double mutant, delivery of CCV cargoes for autophagosome biogenesis is blocked. As a result, clearance of oxidized organelles is impaired, leading to uncontrolled production of secondary ROS and thus to constitutive activation of immunity and ultimately to induction of cell death (right). Note: The coordinated actions of most of the ATG proteins, including ATG2, are required for autophagosome biogenesis.

the ABRC or the Nottingham *Arabidopsis* Stock Center. Homozygous T-DNA insertion mutants were identified by genomic PCR. Transgenic *Arabidopsis* plants expressing GFP-ATG8e in the Col-0 and *atg2-2* backgrounds were described previously (Wang et al., 2011).

Generation of double or triple mutants

The *clc2-1 clc3-1* mutant was crossed with *sid2-2* (Wildermuth et al., 2001), *rbohD* (Torres et al., 2002), and *atg2-1* (SALK_076727) (Yoshimoto et al., 2009; Wang et al., 2011) to generate the respective triple mutants. The primers used to identify the triple mutants by genomic PCR were CLC2-CS808198/SALK_016049-F; CLC2-CS808198/SALK_016049-R; CLC2-GK-T-DNA-LB1; CLC3-CS100219-F; CLC3-CS100219-R; CLC3-sgtDs3′-1; rbohD-dSpm1; rbohD-LP; rbohD-RP; sid2XS691-LP; sid2XS692-RP, sid2-LBal, atg2-1-LP, atg2-1-RP, and LBb1.3. Primer sequences are provided in Supplemental Table 1.

SA quantification

SA was quantified using an Agilent 1260 HPLC system (Agilent Technologies) with a diode array detector, a fluorescence detector, and a column as described previously (Zhang et al., 2017b).

H_2O_2 quantification by DAB staining

H_2O_2 was visualized by DAB staining (Sigma-Aldrich). Detached leaves were placed in DAB solution (1 mg mL^{-1} DAB, pH 5.5) for 2 h, then cleared in 96% (v/v) boiling ethanol for 10 min. H_2O_2 production was detected as a reddish-brown precipitate on the cleared leaves (Ren et al., 2002).

Trypan blue staining

Plant cell death and fungal growth were visualized using trypan blue staining as described previously (Wang et al., 2011).

Carbon and nitrogen starvation treatments

Seeds were germinated and grown on 1/2 MS medium plates supplemented with both C and N (CK) or without C (−C) or N (−N) under normal growth conditions. At 7 days post germination, the +C and −N seedlings were kept under normal growth conditions, and the −C seedlings were placed in the dark to accelerate C deficiency. After dark treatment for 10 days, the −C seedlings were allowed to recover under normal conditions for an additional 10 days, whereas the CK and −N seedlings were grown under normal conditions throughout the entire process. The ingredients for 1/2 MS were 2.2 g/L MS, 0.5 g/L MES, 10 g/L sucrose, and 0.9 g/L Phytoagar. For the −C medium, sucrose was omitted from the 1/2 MS medium. The ingredients for the −N medium were 10 x MS micro mineral mix (Sigma, St Louis), 0.5 x, 3 mM $CaCl_2$, 1.5 mM $MgCl_2$, 1.25 mM KH_2PO_4, 5 mM KCl, 10 g/L sucrose, and 0.9 g/L Phytoagar.

Chlorophyll content measurements

Chlorophyll contents were measured as described previously (Wang et al., 2011). In brief, *Arabidopsis* leaves were extracted by incubation in 1 mL N,N-dimethylformamide for 48 h in the dark at 4°C. Absorbance was recorded at 664 and 647 nm, and total chlorophyll content was calculated and normalized to fresh weight (g) per sample.

Powdery mildew infection

G. cichoracearum strain UCSC1 was maintained by inoculation on *sid2* mutant plants. Six-week-old plants were inoculated with *G. cichoracearum* strain UCSC1, and the resulting symptoms were scored at 7 dpi as described previously (Wang et al., 2011). Trypan blue staining was used to monitor fungal structures and dead cells. The number of conidiophores per colony was counted at 7 dpi. At least 20 colonies were counted for each genotype in one experiment. The experiments were repeated at least three times with similar results.

Pst DC3000 infection

The *Pst* DC3000 infection and HR tests were performed as described previously (Hofius et al., 2009). The bacterial culture at OD_{600} = 1 was diluted to 10^{-4} in 10 mM $MgCl_2$. Four-week-old plants grown under short-day conditions (8-h light/16-h dark) were infiltrated with the bacterial suspension, and bacterial growth was monitored at the indicated dpi.

RNA isolation and RT–qPCR

RNA isolation was performed using TRIzol reagent (ThermoFisher, Shanghai, China). RT–qPCR was performed using an ABI550 Real-Time PCR instrument (Applied Biosystems, Thermo Fisher Scientific) and 2x SYBR Green qPCR Mix (Aidlab, Beijing, China). Sequences of the primers used for RT–qPCR are listed in Supplemental Table 1.

Western blotting

Proteins were prepared from leaves of 4-week-old Col-0, *clc2-1 clc3-1*, and *atg2-1* plants treated in the dark for different times, and the immunoblotting was performed as described previously (Wang et al., 2011). Anti-NBR1 (Agrisera, AS142805) and anti-ATG8 (Agrisera, AS142769) antibodies were used for western blotting.

Yeast two-hybrid assays

The full-length coding sequences of *CLC2*, *CLC3*, and *ATG8a–ATG8i* were amplified from cDNA transcribed from mRNA extracted from *Arabidopsis* seedlings and subsequently cloned into the pGBKT7 (BD) or pGADT7 (AD) vector (Clontech, Mountain View, CA). The primers used for amplification are listed in Supplemental Table 1. Positive interactions were confirmed by growth of the co-transformed yeast on selective medium lacking Trp, Leu, His, and Ade.

Site-directed mutagenesis

The full-length coding sequence of *CLC2* was cloned into the pMD20 T-vector (Takara Bio, San Jose, CA). *CLC2* containing an AIM1 deletion or AIM2 mutation, as well as LDS-mutated ATG8h, were obtained using the Mut Express II Fast Mutagenesis Kit V2 (Vazyme, Nanjing, China) with primers containing the intended mutations. The primers used for amplification are listed in Supplemental Table 1.

Luciferase complementation imaging assay

Full-length coding sequences of *CLC2*, *CLC2-AIM1*, *CLC2-AIM2*, *CLC2-AIM3*, and *ATG8h* or *ATG8i* were cloned into the Firefly Luciferase Complementation Imaging vectors *35S::nLuc* and *35S::cLuc* (Chen et al., 2008) by digestion with BamHI + SalI or KpnI to generate constructs fused with the N-terminal or C-terminal half of luciferase. The primers used for amplification are listed in Supplemental Table 1. The CLC2 and ATG8h fusion construct pairs were co-injected into *N. benthamiana* leaves via agro-infiltration. At 2 days post infiltration, the abaxial surfaces of the infiltrated leaves were sprayed with 1 mM D-luciferin (MedChemExpress, Shanghai, China) and kept in the dark for 7 min to quench the fluorescence. LUC images were captured with a low-light cooled CCD imaging apparatus (Tanon 6600, Biotanon, Shanghai, China).

Confocal microscopy

Transgenic Col-0 and *atg2-2* plants expressing GFP-ATG8e were generated previously (Wang et al., 2011). The *clc2-1 clc3-1* line expressing GFP-ATG8e (*clc2-1 clc3-1/GFP-ATG8e*) was created by crossing with Col-0/*GFP-ATG8e* and screened in the T2 and T3 populations by genomic PCR using the following primers: CLC2-CS808198/SALK_016049-F; CLC2-CS808198/SALK_016049-R; CLC2-GK-T-DNA-LB1; CLC3-CS100219-F; CLC3-CS100219-R; CLC3-sgtDs3′-1; GFP-F; and ATG8e-R. Sequences of the primers are provided in Supplemental Table 1.

Five-day-old transgenic seedlings grown on 1/2 MS medium with or without sucrose were treated in the dark for 2 days, then incubated with or without E-64d, a Cys protease inhibitor that blocks protein degradation in the vacuole (Yoshimoto et al., 2004). Autophagic bodies were visualized by monitoring expression of the GFP-ATG8e fusion protein in the primary roots using a confocal microscope (Zeiss, LSM 880, Oberkochen, Germany) with 488-nm excitation and a 490- to 540-nm band-pass filter set as described previously (Wang et al., 2011). Image processing was performed according to the manufacturer's manual.

GFP-ATG8h, *GFP-ATG8i*, and *CLC2-GFP* fusions were amplified by PCR or over-lapping PCR using the primers listed in Supplemental Table 1. The *35S::GFP-ATG8h*, *35S::GFP-ATG8i*, and *35S::CLC2-GFP* constructs were obtained by cloning the amplified PCR products into the pE1776 vector (Leister et al., 2005). The *35S::GFP-ATG8h* and *35S::GFP-ATG8i* constructs were transformed into Col-0 by the floral dip method (Clough and Bent, 1998). The presence of GFP-ATG8h or GFP-ATG8i in the transgenic *Arabidopsis* seedlings was observed with a confocal laser-scanning microscope (Zeiss, LSM 880, Oberkochen, Germany). *35S::CLC2-GFP* was transiently expressed in *N. benthamiana* leaves by agro-infiltration for a GFP release assay by western blotting as described previously (Xu et al., 2018; Liu et al., 2020).

Co-IP assay

For the Co-IP assay, 3xFlag-ATG8h/CLC2-MBP and 3xFlag-ATG8i/CLC2-MBP were co-expressed in *N. benthamiana* by *Agrobacterium*-mediated transient transformation. At 2 days post infiltration, the leaves were harvested and ground in liquid nitrogen, and proteins were extracted with IP buffer (50 mM Tris–HCl [pH 7.5], 150 mM NaCl, 1 mM EDTA, 5 mM DTT, 0.01% [v/v] Triton X-100, 10 mM PMSF, and 1× protease inhibitor cocktail). Immunoprecipitation was performed using Flag magnetic beads (Bimake, B26101) with gentle rotation at 4°C for 5–6 h. Finally, protein samples were separated by 12% SDS–PAGE. Western blotting was performed with anti-Flag antibody (CWBIO, CW0287M) and anti-MBP antibody (CWBIO, 01254).

CRISPR-Cas9 constructs and plant transformation

Oligos of 20 nucleotides were chosen from the first exon of *ATG8h* (GATTGTTGTCAAGTCTTTCA, 6–25 base pairs [bp] downstream of the ATG start codon of the open reading frame) and the second exon of ATG8i (TAATCGCTAAGTACCCTACT, 59–78 bp downstream of the ATG start codon) (Figure 6A). Both the sense and antisense strands of the chosen oligos were synthesized with ATTG and AAAC that are compatible to Bsa I sticky ends attached to the sense and antisense strands, respectively. The synthesized sense and antisense oligos were mixed in TE buffer and denatured by heating at 98°C for 5 min, followed by annealing at room temperature. The annealed double-stranded oligos were subsequently ligated into the AtU6-26-sgRNA-SK intermediate vector (Yan et al., 2015) predigested with Bsa I. The constructed plasmid was double

digested with the isocaudomers Nhe I and Spe I, and the digested fragment containing the guide sequence was ligated into the pCAMBIA-1300-pYAO:Cas9 destination vector predigested with Spe I and de-phosphorylated with alkaline phosphatase (Yan et al., 2015). The final construct was verified by sequencing. The oligos used for target guide constructs were CRISPR-CAS9-ATG8h-F, CRISPR-CAS9-ATG8h-R, CRISPR-CAS9-ATG8i-F, and CRISPR-CAS9-ATG8i-R. The primers used to identify positive colonies were SK-gRNA-F in combination with CRISPR-CAS9-ATG8h-R or CRISPR-CAS9-ATG8i-R. The primer used for sequencing the intermediate construct was also SK-gRNA-F. The oligos used for positive colony screening in the destination vector were 1300-gRNA-F+CRISPR-CAS9-ATG8h-R and 1300-gRNA-F+CRISPR-CAS9-ATG8i-R. The sequencing primers for the single guide destination vectors were 1300-gRNA-F and 1300-gRNA-R.

For the dual-target (ATG8h + ATG8i) construct, the Nhe I- and Spe I-digested fragment from the intermediate vector containing the ATG8h guide was ligated into the destination vector containing the ATG8i guide predigested with Spe I. Positive clones were identified by colony PCR using CRISPR-CAS9-ATG8i-F and CRISPR-CAS9-ATG8h-R primers. The sequencing primer used for the dual-target destination vector was 1300-gRNA-R. Sequences of the primers are listed in Supplemental Table 1.

The single and dual-target CRISPR-Cas9 constructs were transformed into *Arabidopsis* as described previously (Leister et al., 2005). The positive transgenic plants were first screened on 1/2 MS agar plates containing hygromycin B (30 mg/L), followed by genomic PCR amplification. The ATG8h primer pair and ATG8i primer pair were used for single-target amplifications. The sequencing primers for the amplified genomic fragments were ATG8h-F and ATG8i-F. Sequences of the primers are listed in Supplemental Table 1.

Callose deposition assay and FB1-induced cell death

The callose deposition assay and FB1 (10 μM) infiltration were performed as described previously (Lenz et al., 2011).

Quantification and statistical analysis

Each experiment was repeated at least three times, and representative results are presented. Statistical analyses were performed using SPSS Statistics 27 (Statistical Product and Service Solutions, IBM). The test methods are indicated in the figure legends.

SUPPLEMENTAL INFORMATION

Supplemental information is available at *Plant Communications Online*.

FUNDING

This work was supported by grants from the National Natural Science Foundation of China (32170761, 31571423 and 31371401 to J.-Z.L. and 91754104, 31820103008, and 31670283 to J.P.) and the Iowa State University Plant Sciences Institute and USDA National Institute of Food and Agriculture Hatch project 4308.

AUTHOR CONTRIBUTIONS

J.Z.L., B.J.B., S.A.W., and J.P. conceived the study and designed the experiments. H.J.L., J.R., W.X.W., N.N.W., L.Z., Y.T.Z., M.J.H., M.N., F.L., and N.C. conducted the experiments. J.Z.L. analyzed the data. J.Z.L. wrote the manuscript, and B.J.B., S.A.W., P.A.N., and N.C. revised the manuscript.

ACKNOWLEDGMENTS

We dedicate this paper in memory of our friend and colleague, Prof. Jianwei Pan. His passion for science and fighting spirit will inspire us for years to come. We thank Prof. Dingzhong Tang for kindly providing the *atg2-1* mutant, GFP-ATG8e/Col-0, GFP-ATG8e/*atg2-2* transgenic lines, and *G. cichoracearum* strain UCSC. We also thank Profs. Brian J. Staskawicz, Yule Liu, Sebastian Y. Bednarek, Kewei Zhang, and Chao Wang for generously sharing materials, constructs, and vectors. No conflict of interest declared.

Received: December 17, 2023
Revised: February 2, 2024
Accepted: April 28, 2024
Published: April 30, 2024

REFERENCES

Avin-Wittenberg, T., Michaeli, S., Honig, A., and Galili, G. (2012). ATI1, a newly identified atg8-interacting protein, binds two different Atg8 homologs. Plant Signal. Behav. **7**:685–687.

Baines, K., Yoshioka, K., Takuwa, Y., and Lane, J.D. (2022). The ATG5 interactome links clathrin-mediated vesicular trafficking with the autophagosome assembly machinery. Autophagy Rep. **1**:88–118. https://doi.org/10.1080/27694127.2022.2042054.

Birgisdottir, Å.B., Lamark, T., and Johansen, T. (2013). The LIR motif – crucial for selective autophagy. J. Cell Sci. **126**:3237–3247.

Chen, H., Zou, Y., Shang, Y., Lin, H., Wang, Y., Cai, R., Tang, X., and Zhou, J.M. (2008). Firefly luciferase complementation imaging assay for protein-protein interactions in plants. Plant Physiol. **146**:368–376.

Chen, X., Irani, N.G., and Friml, J. (2011). Clathrin-mediated endocytosis: the gateway into plant cells. Curr. Opin. Plant Biol. **14**:674–682.

Chung, T., Phillips, A.R., and Vierstra, R.D. (2010). ATG8 lipidation and ATG8-mediated autophagy in Arabidopsis require ATG12 expressed from the differentially controlled ATG12a and ATG12b loci. Plant J. **62**:483–493.

Clough, S.J., and Bent, A.F. (1998). Floral dip: a simplified method for Agrobacterium-mediated transformation of Arabidopsis thaliana. Plant J. **16** (6):735–743. https://doi.org/10.1046/j.1365-313x.1998.00343.x.

Devarenne, T.P. (2011). The plant cell death suppressor Adi3 interacts with the autophagic protein Atg8h. Biochem. Biophys. Res. Commun. **412**:699–703.

Gilchrist, D.G. (1997). Mycotoxins reveal connections between plants and animals in apoptosis and ceramide signaling. Cell Death Differ. **4**:689–698.

Gomez, R.E., Chambaud, C., Lupette, J., Castets, J., Pascal, S., Brocard, L., Noack, L., Jaillais, Y., Joubès, J., and Bernard, A. (2022). Phosphatidylinositol-4-phosphate controls autophagosome formation in Arabidopsis thaliana. Nat. Commun. **13**:4385.

Guo, P., Li, Z., Huang, P., Li, B., Fang, S., Chu, J., and Guo, H. (2017). A Tripartite Amplification Loop Involving the Transcription Factor WRKY75, Salicylic Acid, and Reactive Oxygen Species Accelerates Leaf Senescence. Plant Cell **29**:2854–2870.

Guo, Y., Chang, C., Huang, R., Liu, B., Bao, L., and Liu, W. (2012). AP1 is essential for generation of autophagosomes from the trans-Golgi network. J. Cell Sci. **125**:1706–1715.

Hanaoka, H., Noda, T., Shirano, Y., Kato, T., Hayashi, H., Shibata, D., Tabata, S., and Ohsumi, Y. (2002). Leaf senescence and starvation-induced chlorosis are accelerated by the disruption of an Arabidopsis autophagy gene. Plant Physiol. **129**:1181–1193.

Hao, H., Fan, L., Chen, T., Li, R., Li, X., He, Q., Botella, M.A., and Lin, J. (2014). Clathrin and Membrane Microdomains Cooperatively Regulate RbohD Dynamics and Activity in Arabidopsis. Plant Cell **26**:1729–1745.

Hofius, D., Schultz-Larsen, T., Joensen, J., Tsitsigiannis, D.I., Petersen, N.H.T., Mattsson, O., Jørgensen, L.B., Jones, J.D.G., Mundy, J., and Petersen, M. (2009). Autophagic components contribute to hypersensitive cell death in Arabidopsis. Cell **137**:773–783.

Kellner, R., De la Concepcion, J.C., Maqbool, A., Kamoun, S., and Dagdas, Y.F. (2017). ATG8 expansion: a driver of selective autophagy diversification? Trends Plant Sci. **22**:204–214.

Ben Khaled, S., Postma, J., and Robatzek, S. (2015). A Moving View: Subcellular Trafficking Processes in Pattern Recognition Receptor–Triggered Plant Immunity. *Annu.* Rev. Phytopathol. **53**:379–402.

Lamb, C., and Dixon, R.A. (1997). The oxidative burst in plant disease resistance. Annu. Rev. Plant Physiol. Plant Mol. Biol. **48**:251–275.

Lamb, C.A., Dooley, H.C., and Tooze, S.A. (2013). Endocytosis and autophagy: Shared machinery for degradation. Bioessays **35**:34–45.

Lan, H.J., Ran, J., Zhang, L., Wu, N.N., Wang, W.X., Ni, M., Cheng, N., Nakata, P.A., Pan, J., Whitham, S.A., et al. (2023). Clathrin Light Chains are essential in negative regulation of cell death and immunity in Arabidopsis through interacting with autophagy pathway. Preprint at bioRxiv **04.09**, 535952. https://doi.org/10.1101/2023.04.09.535952.

Larson, E.R., Van Zelm, E., Roux, C., Marion-Poll, A., and Blatt, M.R. (2017). Clathrin Heavy Chain Subunits Coordinate Endo- and Exocytic Traffific and Affect Stomatal Movement. Plant Physiol. **175**:708–720.

Leister, R.T., Dahlbeck, D., Day, B., Li, Y., Chesnokova, O., and Staskawicz, B.J. (2005). Molecular genetic evidence for the role of *SGT1* in the intramolecular complementation of Bs2 protein activity in *Nicotiana benthamiana*. Plant Cell **17**:1268–1278.

Lenz, H.D., Haller, E., Melzer, E., Kober, K., Wurster, K., Stahl, M., Bassham, D.C., Vierstra, R.D., Parker, J.E., Bautor, J., et al. (2011). Autophagy differentially controls plant basal immunity to biotrophic and necrotrophic pathogens. Plant J. **66**:818–830.

Li, F., and Vierstra, R.D. (2012). Autophagy: a multifaceted intracellular system for bulk and selective recycling. Trends Plant Sci. **17**:526–537.

Li, F., Zhang, M., Zhang, C., and Zhou, X. (2019). Nuclear autophagy degrades a geminivirus nuclear protein to restrict viral infection in solanaceous plants. New Phytol. **225**:1746–1761.

Liu, F., Hu, W., Li, F., Marshall, R.S., Zarza, X., Munnik, T., and Vierstra, R.D. (2020). AUTOPHAGY-RELATED14 and Its Associated Phosphatidylinositol 3-Kinase Complex Promote Autophagy in Arabidopsis. Plant Cell **32**:3939–3960.

Liu, Y., and Bassham, D.C. (2012). Autophagy: Pathways for self-eating in plant cells. Annu. Rev. Plant Biol. **63**:215–237.

Liu, Y., Schiff, M., Czymmek, K., Tallóczy, Z., Levine, B., and Dinesh-Kumar, S.P. (2005). Autophagy regulates programmed cell death during the plant innate immune response. Cell **121**:567–577.

Macharia, M.W., Tan, W.Y.Z., Das, P.P., Naqvi, N.I., and Wong, S.M. (2019). Proximity-dependent biotinylation screening identifies NbHYPK as a novel interacting partner of ATG8 in plants. BMC Plant Biol. **19**:326.

Marshall, R.S., Hua, Z., Mali, S., McLoughlin, F., and Vierstra, R.D. (2019). ATG8-binding UIM proteins define a new class of autophagy adaptors and receptors. Cell **177**:766–781.e24.

Michaeli, S., Honig, A., Levanony, H., Peled-Zehavi, H., and Galili, G. (2014). Arabidopsis ATG8-INTERACTING PROTEIN1 is involved in autophagy-dependent vesicular trafficking of plastid proteins to the vacuole. Plant Cell **26**:4084–4101.

Nagel, M.K., Kalinowska, K., Vogel, K., Reynolds, G.D., Wu, Z., Anzenberger, F., Ichikawa, M., Tsutsumi, C., Sato, M.H., Kuster, B., et al. (2017). Arabidopsis SH3P2 is an ubiquitin-binding protein that functions together with ESCRT-I and the deubiquitylating enzyme AMSH3. Proc. Natl. Acad. Sci. USA **114**:E7197–E7204.

Neuenschwander, U., Vernooij, B., Friedrich, L., Uknes, S., Kessmann, H., and Ryals, J. (1995). Is hydrogen peroxide a second messenger of salicylic acid in systemic acquired resistance? Plant J. **8**:227–233.

Noda, N.N., Ohsumi, Y., and Inagaki, F. (2010). Atg8-family interacting motif crucial for selective autophagy. FEBS Lett. **584**:1379–1385.

Ohsumi, Y. (2001). Molecular dissection of autophagy: two ubiquitin-like systems. Nat. Rev. Mol. Cell Biol. **2**:211–216.

Paez Valencia, J., Goodman, K., and Otegui, M.S. (2016). Endocytosis and endosomal trafficking in plants. Annu. Rev. Plant Biol. **67**:309–335.

Patel, S., and Dinesh-Kumar, S.P. (2008). Arabidopsis ATG6 is required to limit the pathogen-associated cell death response. Autophagy **4**:20–27.

Ran, J., Hashimi, S.M., and Liu, J.Z. (2020). Emerging Roles of the Selective Autophagy in Plant Immunity and Stress Tolerance. Int J Mol Sci. **21** (17):6321. https://doi.org/10.3390/ijms21176321.

Rao, M.V., and Davis, K.R. (1999). Ozone-induced cell death occurs via two distinct mechanisms in Arabidopsis: The role of salicylic acid. Plant J. **17**:603–614.

Ravikumar, B., Moreau, K., Jahreiss, L., Puri, C., and Rubinsztein, D.C. (2010). Plasma membrane contributes to the formation of pre-autophagosomal structures. Nat. Cell Biol. **12**:747–757.

Ren, D., Yang, H., and Zhang, S. (2002). Cell death mediated by MAPK is associated with hydrogen peroxide production in Arabidopsis. J. Biol. Chem. **277**:559–565.

Rodriguez-Furlan, C., Minina, E.A., and Hicks, G.R. (2019). Remove, recycle, degrade: regulating plasma membrane protein accumulation. Plant Cell **31**:2833–2854.

Rong, Y., Liu, M., Ma, L., Du, W., Zhang, H., Tian, Y., Cao, Z., Li, Y., Ren, H., Zhang, C., et al. (2012). Clathrin and phosphatidylinositol-4,5-bisphosphate regulate autophagic lysosome reformation. Nat. Cell Biol. **14**:924–934.

Seo, E., Woo, J., Park, E., Bertolani, S.J., Siegel, J.B., Choi, D., and Dinesh-Kumar, S.P. (2016). Comparative analyses of ubiquitin-like ATG8 and cysteine protease ATG4 autophagy genes in the plant lineage and cross-kingdom processing of ATG8 by ATG4. Autophagy **12**:2054–2068.

Shirasu, K., Nakajima, H., Rajasekhar, V.K., Dixon, R.A., and Lamb, C. (1997). Salicylic acid potentiates an agonist-dependent gain control that amplifies pathogen signals in the activation of defense mechanisms. Plant Cell **9**:261–270.

Torres, M.A., Dangl, J.L., and Jones, J.D.G. (2002). Arabidopsis gp91phox homologues AtrbohD and AtrbohF are required for accumulation of reactive oxygen intermediates in the plant defense response. Proc. Natl. Acad. Sci. USA **99**:517–522.

Üstün, S., and Hofius, D. (2018). Anti- and pro-microbial roles of autophagy in plant-bacteria interactions. Autophagy **14**:1465–1466. https://doi.org/10.1080/15548627.2018.1475817.

Viotti, C., Bubeck, J., Stierhof, Y.D., Krebs, M., Langhans, M., van den Berg, W., van Dongen, W., Richter, S., Geldner, N., Takano, J., et al. (2010). Endocytic and secretory traffic in Arabidopsis merge in the

trans-Golgi network/early endosome, an independent and highly dynamic organelle. Plant Cell **22**:1344–1357.

Wang, C., Yan, X., Chen, Q., Jiang, N., Fu, W., Ma, B., Liu, J., Li, C., Bednarek, S.Y., and Pan, J. (2013). Clathrin light chains regulate clathrin-mediated trafficking, auxin signaling, and development in Arabidopsis. Plant Cell **25**:499–516.

Wang, P., Pleskot, R., Zang, J., Winkler, J., Wang, J., Yperman, K., Zhang, T., Wang, K., Gong, J., Guan, Y., et al. (2019). Plant AtEH/Pan1 proteins drive autophagosome formation at ER-PM contact sites with actin and endocytic machinery. Nat. Commun. **10**:5132.

Wang, W., Jones, C., Ciacci-Zanella, J., Holt, T., Gilchrist, D.G., and Dickman, M.B. (1996). Fumonisins and *Alternaria alternata lycopersici* toxins: sphinganine analog mycotoxins induce apoptosis in monkey kidney cells. Proc. Natl. Acad. Sci. USA **93**:3461–3465.

Wang, Y., Nishimura, M.T., Zhao, T., and Tang, D. (2011). ATG2, an autophagy related protein, negatively affects powdery mildew resistance and mildew induced cell death in Arabidopsis. Plant J. **68**:74–87.

Wildermuth, M.C., Dewdney, J., Wu, G., and Ausubel, F.M. (2001). Isochorismate synthase is required to synthesize salicylic acid for plant defence. Nature **414**:562–565.

Xu, H.Y., Zhang, C., Li, Z.C., Wang, Z.R., Jiang, X.X., Shi, Y.F., Tian, S.N., Braun, E., Mei, Y., Qiu, W.L., et al. (2018). The MAPK kinase kinase GmMEKK1 regulates cell death and defense responses. Plant Physiol. **178**:907–922.

Yamaguchi, M., Noda, N.N., Nakatogawa, H., Kumeta, H., Ohsumi, Y., and Inagaki, F. (2010). Autophagy-related protein 8 (Atg8) family interacting motif in Atg3 mediates the Atg3-Atg8 interaction and is crucial for the cytoplasm-to-vacuole targeting pathway. J. Biol. Chem. **285**:29599–29607.

Yan, L., Wei, S., Wu, Y., Hu, R., Li, H., Yang, W., and Xie, Q. (2015). High-efficiency genome editing in Arabidopsis using YAO promoter-driven CRISPR/Cas9 system. Mol. Plant **8**:1820–1823.

Yan, X., Wang, Y., Xu, M., Dahhan, D.A., Liu, C., Zhang, Y., Lin, J., Bednarek, S.Y., and Pan, J. (2021). Cross-Talk between Clathrin-Dependent Post-Golgi Trafficking and Clathrin-Mediated Endocytosis in Arabidopsis Root Cells. Plant Cell **33**:3057–3075. https://doi.org/10.1093/plcell/koab180.

Yoshimoto, K., Hanaoka, H., Sato, S., Kato, T., Tabata, S., Noda, T., and Ohsumi, Y. (2004). Processing of ATG8s, ubiquitin-like proteins, and their deconjugation by ATG4s are essential for plant autophagy. Plant Cell **16**:2967–2983.

Yoshimoto, K., Jikumaru, Y., Kamiya, Y., Kusano, M., Consonni, C., Panstruga, R., Ohsumi, Y., and Shirasu, K. (2009). Autophagy negatively regulates cell death by controlling NPR1-dependent salicylic acid signaling during senescence and the innate immune response in Arabidopsis. Plant Cell **21**:2914–2927.

Zhang, Y., Yu, Q., Jiang, N., Yan, X., Wang, C., Wang, Q., Liu, J., Zhu, M., Bednarek, S.Y., Xu, J., Pan, J., et al. (2017a). Clathrin regulates blue light-triggered lateral auxin distribution and hypocotyl phototropism in Arabidopsis. Plant Cell Environ. **40**:165–176.

Zhang, Y., Zhao, L., Zhao, J., Li, Y., Wang, J., Guo, R., Gan, S., Liu, C.J., and Zhang, K. (2017b). *S5H/DMR6* Encodes a Salicylic Acid 5-Hydroxylase That Fine-Tunes Salicylic Acid Homeostasis. Plant Physiol. **175**:1082–1093.

Zhou, J., Ma, J., Yang, C., Zhu, X., Li, J., Zheng, X., Li, X., Chen, S., Feng, L., Wang, P., et al. (2023). A non-canonical role of ATG8 in Golgi recovery from heat stress in plants. Nat. Plants **9**:749–765.

Zhu, X., Ruan, Z., Yang, X., Chu, K., Wu, H., Li, Y., and Huang, Y. (2015). Connexin 31.1 degradation requires the Clathrin-mediated autophagy in NSCLC cell H1299. J. Cell Mol. Med. **19**:257–264.

Zhuang, X., Cui, Y., Gao, C., and Jiang, L. (2015). Endocytic and autophagic pathways crosstalk in plants. Curr. Opin. Plant Biol. **28**:39–47.

Zhuang, X., Wang, H., Lam, S.K., Gao, C., Wang, X., Cai, Y., and Jiang, L. (2013). A BAR-domain protein SH3P2, which binds to phosphatidylinositol 3-phosphate and ATG8, regulates autophagosome formation in Arabidopsis. Plant Cell **25**:4596–4615.